

Reply to the comments of anonymous reviewer #2 on manuscript Entitled " Mixing characteristics of refractory black carbon aerosols determined by a tandem CPMA-SP2 system at an urban site in Beijing"

5 We appreciate very much the patient and insight comments and recommendations of the reviewer in improving this paper and our future research. Here, we will response to all the comments one by one as follows:

General comments:

The paper reports the microphysical properties and aging/ mixing state of rBC particles during summer time in Beijing. The research site is mostly influenced by traffic emissions from the surrounding highways and is well representative of the Beijing urban outflow. Ambient aerosol were measured using the single particle soot photometer (SP2) for 2 weeks (30 May to 13 June 2018). Complementary measurements of O_3 , NO_2 and $PM_{2.5}$ were performed, however, the measurement techniques were not specified in the methodology section, which I recommend to do so.

Reply: The concentrations of $PM_{2.5}$ and gaseous pollutants were from a state control air quality site, provided by the China National Environmental Monitoring Centre. The state control air quality site was 2.5 km from our observation site. We think the air quality condition of the state control site was similar with the air quality condition of our observation site in such close distance. And we added the position of the state control air quality site in Fig. 1b and the measuring instrument type for every pollutants (line 180-183).

20 There were two case studies that the authors refers as 'clean' and 'polluted' for which the rBC properties were determined. Moreover, during these periods, a dedicated experiment was performed by coupling a DMA or CPMA with the SP2 in order to determine the effective density, morphology and absorption enhancement of rBC particles due to coatings. The methods used in this study are valid, however, the measurement setup is questionable. For example, the authors do not mention whether the aerosol particles are dried before detection. The particle size depends on relative humidity (RH) that can strongly influence 25 the results. Note that the RH is much higher in the "polluted" case.

Reply: We add a specific description about the tandem system in a new section to make it more clear, line (145-176). The air sample was dried before it entered into the tandem system. Thus, the RH wouldn't influence the particle size in this study (Fig. 2a).

30 Moreover, I do not agree in using the terms "clean" and "polluted" applied for the two periods. The clean period is rather influenced by the fresh traffic emissions.

Reply: The clean and polluted periods were defined according to the Chinese air quality standard which mainly focus on the mass concentration of $PM_{2.5}$. We agree there is still substantial rBC emission in clean periods. However, there were more

35 pollutant gases and particle matters in polluted periods which may influence the rBC-containing particles' coating and morphology. For example, Zhang et al. (2018) found the D_p/D_c value of rBC-containing particles tended to be larger in the episodes with higher $PM_{2.5}$ mass concentration. That's Why we conducted the tandem experiments separately in clean and polluted episodes.

40 The description of the tandem experiment is not well described and difficult to understand. Since this is one of the highlights of the paper, it deserves a dedicated section on the methodology containing precise information of the measurement period, the atmospheric conditions during the experiment (what kind of air masses were sampled?) and the purposes of doing this. I suggest to have a dedicated section (after section 2.1) in the methodology for the case studies. A table containing the main results of this comparison can be also helpful.

45 Reply: Thanks for the advice, we added a new section to describe the tandem system, (line 145-176).

50 Overall, I suggest improvements of the writing. In my opinion, the discussion of the results are not presented in a precise way and the figure notes are quite vague and lacking information. For all of them, I recommend to give more details, using the full name of the variables.

55 Reply: Thanks for the comments, we will improve our writing in the following version. The figure notes and legends have been improved.

Specific comments:

L149: "In this study, the SP2's low detection bound was set to $D_c = 70 nm$ ". Please re-phrase.

55 Reply: The sentence has been changed to

55 The former : "In this study, the SP2's low detection bound was set to $D_c = 70 nm$." (line 149)

Now: "For rBC with $D_c < 70 nm$, the detect efficiency of SP2 significantly dropped below 60%. Thus, rBC with $D_c < 70 nm$ was not considered in this study." (line 124-126)

L152: Why 1.17 factor was used?

60 Reply: The corrected concentration is : (the measured concentration) / (1-15%) which is the same as (the measured concentration) * 1.17. We have changed the expression:

65 By extrapolating a lognormal function fit to the observed mass distribution, we found that rBC particles outside the detection range caused an ~15% underestimation of the rBC mass concentration. To compensate, the mass concentration of rBC was corrected by dividing by a factor of 0.85 during the measurement. (line 126-129)

L159: replace "owing".

65 Reply: The sentence has been rewritten.

The former: “For rBC-containing particles, the scattering cross section significantly decreased owing to the evaporation of the nonrefractory coating as the rBC core absorbed energy” (line 159)

70 Now: “However, for rBC-containing particles, the particles will evaporate during the measurement since rBC can absorb the laser energy, which results in a decrease in the rBC-containing particles’ sizes and thus a decrease in the σ_{measured} .” (line 108-110)

L171: “The coating density was set to 1.5 g/cm³”. Please re-phrase.

75 Reply: The sentence has been rewritten.

The former: “The coating density was set to 1.5 g/cm³”. (line 171)

Now: “Knowing M_p and M_{rBC} , the scattering cross section of rBC-containing particles can be calculated through Mie-theory with refractive indices of 2.26-1.26i of rBC and 1.48i of coatings, by assuming a core-shell structure and the coating density of 1.5 g/cm³.” (line 172-174)

80 L209: remove “that”.

Reply: We have removed “that” in the text.

L211-212: Which MAC value did you assume for calculating the BC mass? L212: “Overestimation” of? Incomplete sentence.

85 Reply: The discussion about MAAP have been removed in the new manuscript since we found the coatings weren’t the cause of the bias of the rBC mass concentration measured by MAAP and SP2

L218: Rephrase “during which time”.

90 Reply: The sentence have been rewritten.

The former: “A heavy rainfall event occurred from 0300 – 0700LST on June 7, during which time the mass concentration of PM_{2.5} decreased from 65 to 10 $\mu\text{g}/\text{m}^3$ and the mass concentration of rBC decreased from 2.63 to 0.2 $\mu\text{g}/\text{m}^3$.” (line 218)

Now: “On June 7, a heavy rain fall event occurred, most of the major pollutants decreased due to significant wet scavenging. The mass concentration of PM_{2.5} decreased from 65 to 10 $\mu\text{g}/\text{m}^3$ and the mass concentration of rBC decreased from 2.63 to 0.2 $\mu\text{g}/\text{m}^3$ from 0300–0700 LST on June 7.” (line 190-192)

L243 – 260: This whole paragraph discussing “after rain” case should be more concise. It is a bit confusing with presenting several dates. Try to group them.

Reply: Thanks for the advice, we have rewritten the paragraph and make the paragraph more concise. (line 216-221)

L244: What was the decrease in MMD on June 4 in numbers? Is it consistent with the event on June 8?

Reply: The MMD decreased from 186 nm to 170 nm on June 4 and decreased from 183 nm to 159 nm on June 8 (Figure 5). The more decrease of MMD on June 8 may be the result of heavier rain event (Figure 3). We have added the specific MMD number in the paragraph. (line 216)

105

L258: Are the southerly winds representative for the Beijing outflow? And the northerly winds?

Reply: Beijing outflow is mainly affected by the southerly wind and the northerly winds. The north of Beijing is a clean region with little emission while the south of Beijing is one of the most polluted regions in China. We add a detailed discussion about the MMD characteristic when Beijing was affected by the northerly winds to make the result more comprehensive.

110

Since the air mass from the north is always clean, the local rBC emissions may be the main contributors to the total rBC concentration in the northerly wind period. Thus, the MMD may be more influenced by local emissions and show a weak correlation with the wind speed during northerly wind periods. (line 230-234)

L265: Investigation period.

115

Reply: We have changed the expression

L273: "Episode 1", specify the time interval.

Reply: We have specified the time interval in the text.

120

The D_p/D_c distributions for the two episodes before the tandem CPMA/DMA-SP2 experiments are shown in Fig. 7. Episode 1 (June 7 2200 LST – June 8 1200 LST) occurred after a heavy rain period and is representative of a clean condition. Episode 2 (June 11 2300 LST – June 12 1200 LST) was characterized with the highest D_p/D_c value (1.4) and the highest PM_{2.5} concentration value (120 $\mu\text{g}/\text{m}^3$). (line 246-249)

125

L274: "During episode 1, the D_p/D_c distribution exhibited a single peak at 1.05. However, during episode 2, two D_p/D_c distribution peaks were found". What point do you want to make here?

Reply: We want to exhibit the different D_p/D_c distribution during episode 1 and episode 2. We have changed the expression which may be more understandable and concise.

The D_p/D_c exhibited a unimodal distribution during episode 1 and a clear bimodal pattern during episode 2 as shown in the upper panel of Fig. 7. (line 249-250)

130

L285-286: Tends vs. tended.

Reply: Thanks, "tends" seems to be more appropriate.

L304-305: There are more recent studies on the microscopy of BC.

135 Reply: It's true. We update the reference now. (line 282)

L341: "The median MR values of the pollution day were all larger than those on the clean day for the four Mp points. This result demonstrated that rBC had more coating material during the pollution day than the clean day." Couldn't it be related to the higher RH?

140 Reply: A higher RH can truly increase the water content in the rBC-containing particles and thus the size as well as M_R . However, we have dried the rBC-containing particles before the tandem system as shown in Fig. 2(a) to avoid the influence of RH. We will write a new section to introduce the tandem system including the drying process to avoid causing misunderstanding of readers.

145 L380: "indicating in-cloud nucleation scavenging may be a more efficient mechanism for rBC-containing particles". Do you mean removal mechanisms?

Reply: Yes, we will add "removal" to make it more clear.

150 Fig. 1: has four panels. It is helpful for the readers if there is a full description of the measurements (from the top to the bottom) and possibly how they were collected. Moreover, I recommend to indicate the two studied cases in the figure. The same applies for figures 5.

Reply: A new section which is used to describe the tandem system has been added. (line 145-176) and the two studied cases have been indicated in the figure notes of Fig. 2. (line 546-547)

The Fig. 3 has been improved to denote the time when the tandem system was conducted.

155

Fig. 5: Y axis in log scale and increased range. What are the units of $dM/d\log D_c$? The values seem too high!

Reply: Thanks for the advice, we have changed the figure. The unit of $dM/d\log D_c$ has been changed to $\mu\text{g m}^{-3}$.

160 Fig. 7: In the two upper panels, the integral of the area below the curve seems to be larger than 1, is it really the normalized $dN/d\log D_p$? Moreover, the arrows indicating the clean and polluted periods are not precise.

Reply: The former normalized $dN/d\log D_p$ was obtained by letting the maximum value of the histogram be 1. We have changed the calculation to let the integral of the area be 1.

The arrows have been in bold to make them more clear and extra guide line have been added to denote the clean and polluted periods.

165

Fig. 8: Where are the Ox measurements from?

Reply: The concentrations of $\text{PM}_{2.5}$ and gaseous pollutants were from a state control air quality site, provided by the China National Environmental Monitoring Centre. The state control air quality site was 2.5 km from our observation site. We think

the air quality data is similar in such close distance. And we added the position of the state control air quality site in Fig. 1b.

170 (line 186-189)

Fig. 9: Relationship between effective density and mobility diameter of?

Reply: We have made the figure note more specific. Now:

Relationship between effective density and mobility diameter of rBC-containing particles. The black circle and triangle denote

175 the fresh rBC-containing particles ($D_p/D_c = 1$) measured in clean day and polluted day in this study. Other markers denote the data from previous research. (line 576-579)

Fig. 11: MR = mass ratio of non-refractory matter to rBC. Add the full name to the figure description.

Reply: We have followed your advice. (line 584)

180

Figure S1: Does the ‘after experiment’ calibration have only one data point? Try to use different markers so that both measurements are visible on the plot.

185 Reply: Yes, there is only one data point. The purpose of this calibration is to determine the laser intensity of SP2. In fact, the DMT company suggests the calibration of the scattering signal only needs one data point. Thus, we only did calibration of scattering signal using PSL with diameter of 240 nm after the experiment which showed good consistency with the calibration before the experiment (varied within 3%) demonstrating the stability of the instrument.

Fig. S7: This figure is important to understand the origin of air masses for the two study cases. However, there is no information of the age or the starting point of the back trajectories. Also please adjust the scale of the plot.

190 Reply: We have drawn this figure again and specifically describe the calculation of the trajectories. (Section 2 in Supplementary, line 45-54).

195 Zhang, Y. X., Zhang, Q., Cheng, Y. F., Su, H., Li, H. Y., Li, M., Zhang, X., Ding, A. J., and He, K. B.: Amplification of light absorption of black carbon associated with air pollution, *Atmospheric Chemistry and Physics*, 18, 9879-9896, 10.5194/acp-18-9879-2018, 2018.

200 **Reply to the comments of anonymous reviewer #3 on manuscript Entitled " Mixing
characteristics of refractory black carbon aerosols determined by a tandem CPMA-SP2
system at an urban site in Beijing"**

We appreciate very much the patient and insight comments and recommendations of the reviewer in improving this paper and our future research. Here, we will response to all the comments one by one as follows:

205 General comments:

First, a full and careful proofreading is necessary to catch all the grammar and word choice errors. I have listed a bunch, but am not confident I listed them all here. In fact, after a while, I gave up listing them because this was taking too much time. Please correct these errors before sending out for review again.

210 Reply: Great thanks to the reviewer to point out the grammar errors. We have changed the error places and checked the manuscript several times again.

215 Second, there needs to be better quantification of the SP2 calibrations. To give this dataset importance in terms of the big picture, better uncertainties are necessary. The conclusions all sound reasonable as far as I can tell; but they need to be mathematically rigorous as well.

Reply: We have determined the uncertainty of our SP2 and the error bars have been added to the calibration figures. Also, the uncertainties of some key parameters have been evaluated.

220 A final big comment, there are many places in the paper that need more detail and clarifications. See my many comments listed below. In general, a better description of the tandem experiments and of the models used to calculate absorption enhancements are necessary. Many other places need rewording for clarity.

225 Reply: We have reorganized the method section and added a part to describe the tandem system including the configuration, time, the air mass during the tandem system (Section 2.32 and line 145-176 in the manuscript). The description of the calculation of absorption enhancement (Section 3 in supplementary) is added in the supplementary. Many parts of the manuscript have been rewritten to make it clearer.

Specific comments:

230 Line 21 - Is "enhancing rate" standard terminology? I don't know what the units are (0.013 what per hour?).

Reply: 1) We changed the expression of “enhancing rate” to “growth rate”.

2) D_p/D_c is a dimensionless quantity, so there shouldn’t be a unit for 0.013. We change to report the growth rate of D_p instead of D_p/D_c to make it clearer for readers. The growth rate of D_p now has a unit of “nm”. (line 21)

235 **Line 21 - Should the “x” be a subscript in “Ox”?**

Reply: Thanks, we have changed the mistake. (line 21)

Line 65 - Is the “18.97%” number really accurate to two decimal places?

Reply: We directly cited this value from the work of (Qin and Xie, 2012), so we think it’s not appropriate to change the value which we cited.

Line 95 - I don’t understand the sentence beginning with “Anthropogenic”.

Reply: We have changed the expression to make it clearer. What we mean is the emission in the campus is little, which led little influence of the observation site. Now:

245 **Anthropogenic emissions from the experimental campus were negligible. Thus, this site can well represent the urban conditions in Beijing. (line 89-90)**

Line 99 - A few more details would be nice on Fig 2a - what is the residence time in the diffusion dryer? Did you check if there were any particle losses in the dryer? When switching configurations, how long did you wait for the sampling to stabilize?

Reply: 1) Good advice, we would like to check such loose and correct the concentration according to the probable particle loose in the diffusion dryer. Unfortunately, our SP2 has some problems now and have been sent to the manufacturers for repairing and we can’t do the test at present.

2) We waited a long time (about half an hour) after changing the regular single SP2 observation to tandem system measurement. And waiting for about 2 min every time we change the setpoint of DMA/CPMA to let the system stabilize, we have added these details in the method section. (line 156, line 168).

Line 104-105 - Should show error bars/scatter in the data on Fig S1. Also should quantify how constant the laser was during the study. Also, be careful of wording – two data points does not ensure that the laser was constant during the study, just that the beginning and end points were similar. Without more data, it even looks like intensity may have been drifting in one direction.

Reply: 1) There is a parameter called YAG power which is recorded in the housekeeping file in SP2 and reflects the laser intensity. We found the YAG power was 4.8 ± 0.1 during the observation indicating the stable condition of the laser.

265 2) Yes, we agree that two data points does not ensure that the laser was constant. We reword the expression and use YAG power to prove the laser was nearly constant during the study. Now:

The calibration of the scattering channel and incandescence channel was also conducted after the observation, the calibration coefficient varied little (<3%) and the YAG power (laser intensity index recorded by SP2) fluctuated with 4.8 ± 0.1 indicating the stable condition of SP2 during the observation period. (line 119-121)

270

Line 115 - Is it useful? (Don't use "could be".)

Reply: We have changed the expression.

275 Line 117 - Can you estimate uncertainty from your own calibration of the SP2? You should be able to, especially with a CPMA.

Reply: Yes, we have determined the uncertainty of our own SP2 and reported in the manuscript. (line 105)

280 Line 121 - Is Fig S2 really necessary? Line 123 - Is it really necessary to quote the CPMA force balance equation? What does your study do with this equation specifically? Line 127 - Is the comment about superiority of the CPMA relative to the APM necessary? What value does this statement add to your study specifically?

Reply: We have removed the Fig S2 and simplified the introduction of CPMA to make the paper more concise.

285 Line 136 - More precisely, the peak LII signal is what is used, not the entire LII signal.

Reply: Yes, we have changed the expression. Now:

The LII peak- M_{rBC} relationship is thus obtained (Fig. S1). (line 104)

290 Line 137 - Why did you use a spline fit when earlier you state that there is a linear relationship between peak height and rBC mass?

295 Reply: It's nearly linear relationship between LII peak height and rBC mass, but not perfectly linear. The DMT company suggested their custom to use a spline fit. The coefficient of the spline fit is exhibited in Fig S1. In fact, the coefficient of x^2 is very small.

Figure S3 - Should show error bars showing the scatter in the data and uncertainty in the particle mass from the CPMA. Also, if there is no calibration equation, how do you use these data?

Figure S5 - Again, would be nice to see error bars showing scattering/uncertainty in the data.

300

Reply: We have followed the advice of the reviewer. Now, the error bar and calibration equation are exhibited on the figure. (Fig S1-S3)

Line 138 - What does “approximately” mean? You should quantify these fits. And be more clear - these are spline fits like in
305 Fig S3? My same comments apply to Fig S4 as above for S3 (include error bars, etc.).

Reply: The coefficient of DMA-SP2 calibration and CPMA-SP2 calibration varied little (<3%). For conciseness, we don’t mention the DMA-SP2 calibration since the coefficient used in this study came from the CPMA-SP2 calibration.

310 Line 152 - Why multiply by 1.17 and not 1.15?

Reply: The corrected concentration is: (the measured concentration) / (1-15%) or (the measured concentration) * 1.17. We have changed the expression to “dividing by a factor of 0.85”. We have changed the expression, now:

315 By extrapolating a lognormal function fit to the observed mass distribution, we found that rBC particles outside the detection range caused an ~15% underestimation of the rBC mass concentration. To compensate, the mass concentration of rBC was corrected by dividing by a factor of 0.85 during the measurement. (line 128-129)

Line 159 - This whole section should probably be edited for clarity. Specifically here, I don’t understand “dividing by laster intensity”. Line 161 - Again, clarity - reword “the data before a length”

320

Reply: We have reworded the method section to make it clearer.

Line 173 - How did you determine which was the most proper refractive index to use? Supplemental - What is “RCT”?

325 Reply: We have removed this part and directly use the refractive index from the previous research.

Line 182 - To be clear, the M_{rBC} is what is measured by the SP2, correct? Section 2.3.3 needs some work for clarity.

Reply: Yes, it’s directly measured by SP2. The method section has been rewritten.

330

Line 192 - Again, there is no quantification of how well the current study compares with previous studies. It looks like your data points are systematically higher than the polynomial fit by Gysel. You should quantify the relationship and tell the reader what it means for your study.

335 Reply: Our results are ~7% higher than the poly-fit of Gysel but lower than the results from Moteki and Kondo. These differences may be result of different characteristics of Aquadag with varied lot and different instrument condition (such as the uncertainty of SP2).

340 Line 195 - What is the purpose of Section 2.3.5? Need more details. Where exactly do the parameters going into the Mie model come from? The Cabs variables should be defined in Table S1.

Reply: We have rewritten the method section and added a new section in the supplementary to describe the optical calculation. (Section 3 in supplementary)

345 Line 202 - What instruments measured the gaseous pollutants? Line 207 - What measured total PM_{2.5} mass? Was this measurement behind the cyclone? If so, was the cyclone's cut size at 2.5 microns, or something higher? These details might effect your measurement.

350 Reply: The concentrations of PM_{2.5} and gaseous pollutants were from a state control air quality site, provided by the China National Environmental Monitoring Centre. The state control air quality site was 2.5 km from our observation site. We think the air quality data is similar with the air quality of our observation site in such close distance. And we added the position of the state control air quality site in Fig. 1b. (line 180-183)

355 Line 210 - Should provide details on the MAAP in the method section. Line 213 - What do you mean "may be affected by coating"? With the instrumentation you have, you should be able to unambiguously determine if the coatings are the reason for the discrepancy. That analysis could be an important part of this work.

360 Reply: Thanks. It's a good advice to examine whether the coatings are the reason for the discrepancy. We did the test and found there wasn't strong relationship between the coating thickness and the discrepancy between MAAP and SP2. Thus, we remove the part of MAAP in the manuscript.

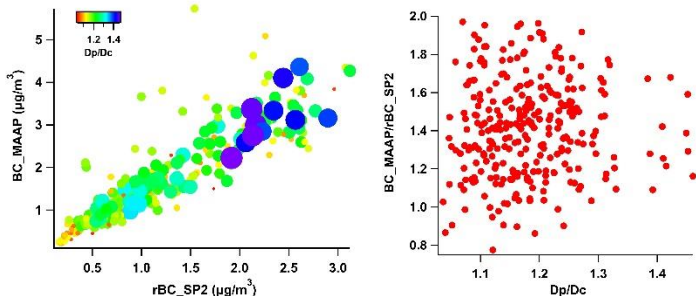


Figure 1 (a) The relationship between the mass concentration of BC (rBC) measured by MAAP and SP2, the color denoted the coating thickness. (b) The relationship between the coating thickness and the ratio of mass concentration measured by SP2 and MAAP.

Line 213 - Maybe start a new paragraph with the sentence beginning with “During”? This paragraph is a bit haphazard and should be rewritten probably.

370 Reply: Thanks, we changed the expression of this paragraph.

Line 216 - You don't specifically reference the other parts of Fig 3 - you should.

375 Reply: We try to describe more in revised version but not too much because the main purpose of this paper is to explore the properties of rBC. This Figure aimed to provide a basic observation condition for the readers.

Fig S9 - Need numbers of your scale bars. Line 223 - Why is June 13 not shown in Fig S9?

380 Reply: We have drawn Fig S9 again and added the backward trajectories of June 13 on Fig S9. Now: Figure S5 in supplementary.

Line 223 - To this point, I still don't understand what “the tandem CPMA-DMA-SP2 experiment” is. There are a lot more details and description needed in the Methods.

385 Reply: We have rewritten the method and added a new section to describe the tandem experiment. (line 145-176)

Line 276 - It actually looks like the increase was on June 12, not June 13.

Reply: Yes, it's on June 12. The episode 2 that we referred here is just June 12. We conducted the tandem experiment on June 13. So, the D_p/D_c value from single SP2 measurement is only available on June 12. And we report the D_p/D_c before the tandem experiment. The expression of this part has been modified. Now:

The D_p/D_c distributions for the two episodes before the tandem CPMA/DMA-SP2 experiments are shown in Fig. 7. Episode 1 (June 7 2200 LST – June 8 1200 LST) occurred after a heavy rain period and is representative of clean conditions. Episode 2 (June 11 2300 LST – June 12 1200 LST) was characterized by the highest D_p/D_c value (1.4) and the highest $PM_{2.5}$ concentration value ($120 \mu\text{g}/\text{m}^3$) during the observation period. (line 246-249)

Line 277 - Where does 63% come from?

Reply: 63% is cited from (Zhang et al., 2018). The air quality in Beijing is easily influenced by the regional pollution transportation in pollution conditions (Wu et al., 2017; Li et al., 2017). We just use this number in the previous research to demonstrate our inference that the rBC-containing particles with $D_p/D_c = 1.8$ in the right peak of the bimodal distribution may be the result of transportation from pollution region.

Line 295 - Do you have any idea the magnitude/emission rate of fresh rBC in Beijing? If so, you could use that number for a closure study.

Reply: It's a good advice. It's possible to estimate the true growth rate of D_p by simultaneously considering the fresh rBC emission and the "apparent" D_p growth rate. And this true growth rate value is important in the atmospheric model. Unfortunately, the emission data about the aging degree of rBC from different emission sectors is still lacking. We may conduct laboratory experiments to determine the rBC aging degree from varied rBC sources and try to estimate the true D_p growth rate in the future.

Line 305 - This sentence is worded as if the Li et al 2003 study took images of the rBC from this study, which is obviously not correct. Were any new microscopy images taken from the current study period?

Reply: There was no new microscopy images taken from current study. The literature cited here is to support the argument that bare rBC is in a fractal structure. We have changed the expression to make it clearer and added some new literatures. Now: This significant discrepancy indicates bare rBC was in a fractal structure consistent with the previous research from electron microscopic image that bare rBC was in a fractal chain-like structure (Li et al., 2003; Adachi and Buseck, 2013; Wang et al., 2017). (line 285-286)

Line 325 - What ambient measurements? From Peng et al 2016? These effective densities are nothing like what you report in the previous section.

425 Reply: Yes, it's from Peng et al 2016, we cite this literature in order to support the argument that the rBC-containing particles tend to become more compact with the coating increasing. The effective densities are the parameters in Peng's literature to support this argument. However, we think this sentence may confuse the readers and thus we changed the expression in the manuscript. Now:

430 Different techniques have been used to explore the morphology of rBC-containing particles in ambient and laboratory measurements (Zhang et al., 2008; Peng et al., 2016; Pagels et al., 2009). It is generally agreed that the morphology of rBC-containing particles will become more compact with the aging process or with increasing coating thickness. (line 310-312)

Line 363 - Did you find the large uncertainty? Or did Liu et al 2017? Discuss more.

435 Reply: Yes, both of our study and Liu found the uncertainty, typically in the external and transit stage because of the assumption in the morphology-dependent model. The section about the light absorption have been rephrased.

Line 366 - What is the “morphology dependent model”? I am very confused by the whole Section 4.2.2.

440 Reply: We rephrase this section and specifically describe the morphology-dependent model in the supplementary.

Line 380 - More efficient than what?

Reply: What we mean is the wet scavenging may be a more efficient removal mechanism for larger rBC-containing particles.

445 We have changed the expression. Thanks for reminding.

Technical corrections

Great thanks for the patient and careful comments about the technical corrections from the reviewer, we have corrected the 450 technical corrections pointed by the reviewer and carefully checked the manuscript again and again. Thanks again for the reviewer for improving this paper.

Line 44 - should be “into the atmosphere”

Line 45 - need a comma after condensation

455 Reply: Now: After being emitted into the atmosphere, BC particles tend to mix with other substances through coagulation, condensation, and other photochemical process, which significantly changes BC's cloud condensation nuclei activity as well as its light absorption ability (Liu et al., 2013; Bond and Bergstrom, 2006). (line 41-44)

Line 83-84 - reword: the data are not analyzed in the discussion section, they are presented

460 Reply: Now: A tandem experiment combining a centrifugal particle mass analyzer (CPMA, Cambustion Ltd.) and a differential mobility analyzer (DMA, model 3085A, TSI Inc., USA) with a SP2 were performed during two typical cases, focusing on BC-containing particles' microphysical properties. (line 76-78)

Line 86-87 - reword "incandescent signal emissions"

465 Reply: Now: After a rBC-containing particle crosses the beam, it is heated to incandesce by sequentially absorbing the laser power. (line 93-95)

Line 87 - What is "this rule"?

Reply: What we mean is we would use rBC as the abbreviation in the following section. Now:

470 For the SP2, the mass concentration of BC was measured on the basis of incandescent signal emissions; therefore, refractory black carbon (rBC) was used. (line 81-82)

Line 95 - Fig 1b, specifically

Reply: Thanks, we have changed. (line 89)

475 Line 104 - reword: the laser intensity is not constant by performing PSL calibrations
Reply: We use a YAG power index in the housekeeping file to support the stability of our SP2. Yes, it's not constant. We rephrase the expression, now:

480 The calibration of the scattering channel and incandescence channel was also conducted after the observation, the calibration coefficient varied little (<3%) and the YAG power (laser intensity index recorded by SP2) fluctuated with 4.8 ± 0.1 indicating the stable condition of SP2 during the observation period. (line 119-121)

Line 148 - unified should be unity; low should be lower

Reply: Now:

485 For large particles, the SP2 detection efficiency was approximately unity and decreased gradually for smaller rBC particles (Fig. S3). (line 123-124)

Line 151 - without should be outside

Reply: Now:

490 By extrapolating a lognormal function fit to the observed mass distribution, we found that rBC particles outside the detection range caused an ~15% underestimation of the rBC mass concentration. (line 126-128)

Line 156 - is intracavity a noun?

Line 164-165 - reword “description ... described”

495 Line 170 - the densities are not defined in the text nor in Table S1

Line 174 - add “respectively” to the sentence

Line 179 - reword

Reply: These sentences have been deleted in the method section in the new manuscript.

500 Line 205 – reword

Reply: Former: O₃ dominant pollution occurred at 1400 LST on June 2, with a maximum of 145 ppbv, reflecting high atmospheric oxidant levels and strong photochemistry during the observation.

Now: The maximum O₃ concentration appeared at 1400 LST on June 2 with a value of 145 ppbv, reflecting high atmospheric oxidant levels and strong photochemistry during the observation. (line 185)

505

Line 207 - Don't use “this” as the subject of a sentence.

Reply: Former: The mass concentration of rBC was $1.21 \pm 0.73 \mu\text{g}/\text{m}^3$ on average, accounting for $3.5 \pm 2.4\%$ of PM_{2.5} on an hourly basis. This was comparable to the previous filter-based measurement in Beijing, with an average fraction of 3.2% in the summer of 2010 (Zhang et al., 2013)."

510

Now: The mass concentration of rBC was $1.21 \pm 0.73 \mu\text{g}/\text{m}^3$ on average, accounting for $3.5 \pm 2.4\%$ of PM_{2.5} on an hourly basis, which was comparable to the previous filter-based measurement in Beijing, with an average fraction of 3.2% in the summer of 2010 (Zhang et al., 2013). (line 186-188)

Line 209-210 - reword, I don't think this is actually a sentence

515

Reply: It has been deleted.

Line 232 - MED or MMD?

Reply: It's MED. Liu et al. (2014) only reported the average MED and standard deviation of MED in winter and summer but not MMD, but these MED value also show a summer-low-winter-high trend.

520

Line 242 - combination should be combined

Reply: Now:

525 The diurnal cycle reached a peak plateau between 0300–0700 LST and it decreased gradually in the afternoon, which was controlled by the combined effects of the development of a planetary boundary layer (PBL) variation and on-road rBC emissions. (line 213-215)

Line 243 – reword

530 Reply: Former: “Significant change of rBC’s mass size distribution occurred on June 7, corresponding to the heavy rain period. After the heavy rain event, the MMD decreased sharply to 159 nm. This decreasing trend of MMD also occurred on June 4 during another rainfall event.”

Now: After the two rain events (June 4 and June 7) as shown in Fig. 3, the MMD decreased significantly from 186 nm to 170 nm and from 183 nm to 159 nm separately. (line 216-217)

535

Li, J., Du, H., Wang, Z., Sun, Y., Yang, W., Li, J., Tang, X., and Fu, P.: Rapid formation of a severe regional winter haze episode over a mega-city cluster on the North China Plain, *Environ Pollut*, 223, 605-615, 2017.

540 Liu, D., Allan, J. D., Young, D. E., Coe, H., Beddows, D., Fleming, Z. L., Flynn, M. J., Gallagher, M. W., Harrison, R. M., Lee, J., Prevot, A. S. H., Taylor, J. W., Yin, J., Williams, P. I., and Zotter, P.: Size distribution, mixing state and source apportionment of black carbon aerosol in London during wintertime, *Atmospheric Chemistry and Physics*, 14, 10061-10084, 10.5194/acp-14-10061-2014, 2014.

Pagels, J., Khalizov, A. F., McMurry, P. H., and Zhang, R. Y.: Processing of Soot by Controlled Sulphuric Acid and Water Condensation Mass and Mobility Relationship, *Aerosol Science and Technology*, 43, 629-640, Pii 910341827 10.1080/02786820902810685, 2009.

545 Peng, J. F., Hu, M., Guo, S., Du, Z. F., Zheng, J., Shang, D. J., Zamora, M. L., Zeng, L. M., Shao, M., Wu, Y. S., Zheng, J., Wang, Y., Glen, C. R., Collins, D. R., Molina, M. J., and Zhang, R. Y.: Markedly enhanced absorption and direct radiative forcing of black carbon under polluted urban environments, *P Natl Acad Sci USA*, 113, 4266-4271, 10.1073/pnas.1602310113, 2016.

550 Qin, Y., and Xie, S. D.: Spatial and temporal variation of anthropogenic black carbon emissions in China for the period 1980-2009, *Atmospheric Chemistry and Physics*, 12, 4825-4841, 10.5194/acp-12-4825-2012, 2012.

Wu, J. B., Wang, Z. F., Wang, Q., Li, J., Xu, J. M., Chen, H. S., Ge, B. Z., Zhou, G. Q., and Chang, L. Y.: Development of an on-line source-tagged model for sulfate, nitrate and ammonium: A modeling study for highly polluted periods in Shanghai, China, *Environ Pollut*, 221, 168-179, 10.1016/j.envpol.2016.11.061, 2017.

555 Zhang, R. Y., Khalizov, A. F., Pagels, J., Zhang, D., Xue, H. X., and McMurry, P. H.: Variability in morphology, hygroscopicity, and optical properties of soot aerosols during atmospheric processing, *P Natl Acad Sci USA*, 105, 10291-10296, 10.1073/pnas.0804860105, 2008.

Zhang, Y. X., Zhang, Q., Cheng, Y. F., Su, H., Li, H. Y., Li, M., Zhang, X., Ding, A. J., and He, K. B.: Amplification of light absorption of black carbon associated with air pollution, *Atmospheric Chemistry and Physics*, 18, 9879-9896, 10.5194/acp-18-9879-2018, 2018.

560

Mixing characteristics of refractory black carbon aerosols at an urban site in Beijing

565 Hang Liu^{1,2}, Xiaole Pan¹, Dantong Liu³, Xiaoyong Liu^{1,4}, Xueshun Chen¹, Yu Tian¹, Yele Sun^{1,2,4},
Pingqing Fu⁵, Zifa Wang^{1,2,4}

¹ State Key Laboratory of Atmospheric Boundary Layer Physics and Atmospheric Chemistry, Institute of Atmospheric Physics, Chinese Academy of Sciences, Beijing, 100029, China

² University of Chinese Academy of Sciences, Beijing, 100049, China

³ Department of Atmospheric Sciences, School of Earth Sciences, Zhejiang University, Hangzhou, Zhejiang, 310027, China

570 ⁴ Center for Excellence in Regional Atmospheric Environment, Chinese Academy of Science, Xiamen, 361021, China

⁵ Institute of Surface-Earth System Science, Tianjin University, Tianjin 300072, China

Correspondence to: Xiaole PAN (panxiaole@mail.iap.ac.cn)

Abstract Black carbon aerosols play an important role in climate change because they directly absorb solar radiation. In this

575 study, the mixing state of refractory black carbon (rBC) at an urban site in Beijing in the early summer of 2018 was studied with a single particle soot photometer (SP2) as well as a tandem observation system with a centrifugal particle mass analyzer (CPMA) and a differential mobility analyzer (DMA). The results demonstrated that the mass-equivalent size distribution of rBC exhibited an approximately lognormal distribution with a mass median diameter (MMD) of 171.2 nm. When the site experienced prevailing southerly winds, the MMD of rBC increased notably, by 19%. During the observational period, the 580 ratio of the diameter of rBC-containing particles (D_p) to the rBC core (D_c) was 1.20 on average for $D_c=180$ nm, indicating that the majority of rBC particles were thinly coated. The D_p/D_c value exhibited a clear diurnal pattern, with a maximum at 1400 LST and a D_p growth rate of 2.34 nm/h; higher O_x conditions increased the coating growth rate.

The microphysical properties of rBC was also studied. Bare rBC particles were mostly found in fractal structures with a mass fractal dimensions (D_{fm}) of 2.35 with limited variation during both clean and polluted periods. The morphology of rBC changed 585 with coating thickness increasing. rBC-containing particles were primarily found in external fractal structures when the mass ratio of nonrefractory matter to rBC (M_R) < 1.5, and they changed to a core-shell structure when $M_R > 6$, at which point the measured scattering cross section of rBC-containing particles was consistent with that based on the Mie scattering simulation.

We found that only 28% of the rBC-containing particles were in core-shell structures with a particle mass of 10 fg on clean 590 period but that proportion increased considerably, to 45%, on polluted period. Due to the morphology change, the absorption enhancement (E_{abs}) was 11.7% lower than that predicted for core-shell structures.

1 Introduction

Black carbon (BC) aerosol is one of the principal light-absorbing aerosols in the atmosphere. BC is regarded as one of the most important components contributing to global warming (Bond et al., 2013). BC has a much shorter lifetime than CO₂.

595 Thus, BC's radiative perturbation on a regional scale may be different from globally averaged estimates. It has been reported that BC's direct radiative forcing can reach an order of +10 W m⁻² over East and South Asia (Bond et al., 2013). BC aerosols can also influence the climate by altering cloud properties, such as the evaporation of cloud droplets, cloud lifetime and albedo (Ramanathan et al., 2001;Ramanathan and Carmichael, 2008). Ding et al. (2016) determined that the existence of BC in the upper mixing layer could absorb downward solar radiation, impeding the development of the boundary layer, which aggravates air pollution. Moreover, BC aerosols have detrimental health effects. BC and organic carbon are regarded as the most toxic pollutants in PM_{2.5} and lead to as many as ~3 million premature deaths worldwide (Adler et al., 2010;Apte et al., 2015).

600 BC is typically emitted from the incomplete combustion of fossil fuels and biomass. After being emitted into the atmosphere, BC particles tend to mix with other substances through coagulation, condensation, and other photochemical processes that significantly change BC's cloud condensation nuclei activity as well as its light absorption ability (Bond et al., 2013;Liu et al., 2013).

605 The model results suggest that after BC's core is surrounded by a well-mixed shell, its direct absorption radiative forcing could be 50% higher than that of BC in an external mixing structure (Jacobson, 2001). Such an absorption enhancement phenomenon is interpreted as exhibiting a “lensing effect”, in which a non-absorbing coating causes more radiation to interact with the BC core and thus more light is absorbed. This absorption enhancement effect has been proven in laboratory studies (Schnaiter et al., 2005). Shiraiwa et al. (2010) reported that the absorption enhancement of BC in a core-shell structure increased with coating thickness and reached a factor as high as 2. Nevertheless, field observation results demonstrated large discrepancies (6 to 40%) in the absorption enhancement of aged BC particles (Cappa et al., 2012;Lack et al., 2012). The discrepancies could be attributed to the complex mixing state of BC in the real atmosphere, which depends on the coating composition, the coating amount and the size of the BC core and structure. Bond et al. (2013) regarded the mixing state of BC as one of the most important uncertainties in evaluating BC direct radiative forcing. Furthermore, freshly emitted BC is initially 610 hydrophobic. Mixing BC with other soluble materials will significantly increase BC-containing particles' hygroscopicity and thus their ability to become cloud condensation nuclei (Bond et al., 2013;Popovicheva et al., 2011). This ability is associated with the wet deposition rate and consequently influences the lifetime and spatial distribution of BC particles in the atmosphere. For these reasons, more observations are needed to determine the specific spatial and temporal distribution of BC's mixing state, which would be helpful for minimizing the uncertainty in evaluating BC's climatic and environmental effects.

615 China's economy has grown rapidly in recent decades, accompanied by the substantial emission of pollutant precursors. Annual emissions of BC in China are reported to have increased from 0.87 Tg in 1980 to 1.88 Tg in 2009, comprising half of the total emissions in Asia and an average of 18.97% of the global BC emissions during this period (Qin and Xie, 2012). Such substantial BC emissions greatly influence the regional climate and environment (Ding et al., 2016;Menon et al., 2002). Although temporal/spatial variations in BC and the corresponding optical properties of aged BC have been recently reported

625 (Cao et al., 2007; Cao et al., 2004; Zhang et al., 2009), the number of observational studies on BC's mixing state remains insufficient. Recently, single particle soot photometer (SP2) has been used as a reliable instrument for estimating the mixing state of BC due to its single particle resolution and high accuracy. Several studies have used SP2 to investigate BC's mixing state in China (Gong et al., 2016; Huang et al., 2012; Wang et al., 2016; Wu et al., 2017). Most studies have primarily focused on the variability of BC's mixing state on severe haze days during winter because of the extremely high concentrations of
630 particle matter and low visibility. In summer, higher radiation and high hydroxyl radical concentrations favor photochemical reactions and thus contribute to the condensation aging of BC. By using a smog chamber, Peng et al. (2016) found that the amount of BC-containing particles increased rapidly owing to the photochemical aging of the BC coating materials from Beijing's urban environment, even in relatively clean conditions. Cheng et al. (2012) noted that the changing rate of BC from an external to internal mixing state can reach up to 20% / h in summer. Thus, the mixing state of BC should also be carefully
635 considered on relatively clean days during summer.

In this study, we used an SP2 to investigate BC in the urban areas of Beijing, China, during early summer, focusing on the size distribution and mixing state of BC-containing particles. **Field experiments using a tandem system consisting of a centrifugal particle mass analyzer (CPMA, Cambustion Ltd.) and a differential mobility analyzer (DMA, model 3085A, TSI Inc., USA) with an SP2 were performed during two typical cases, focusing on BC-containing particles' microphysical properties.** Various
640 techniques have been developed to quantify the mass concentration of BC aerosols, including optical, thermal, thermal-optical and photoacoustic methods. **For the SP2, the mass concentration of BC was measured on the basis of incandescent signal emissions; therefore, refractory black carbon (rBC) was used.** The abbreviations and symbols used in this paper are listed in Table S1.

2 Observation and methodology

645 2.1 Site description

The measurement of rBC particles was performed from May 30 to June 13, 2018, in an air-conditioned container located in the tower campus of the State Key Laboratory of Atmospheric Boundary Layer Physics and Atmospheric Chemistry, Institute of Atmospheric Physics (LAPC, longitude: 116.37°E; latitude: 39.97°N). The sampling site is located between the northern third and fourth ring roads of Beijing, approximately 50 m from the closest road and 380 m away from the nearest highway
650 (the Jingzhang highway) (Fig. 1b). **Anthropogenic emissions from the experimental campus were negligible. Thus, this site can well represent the urban conditions in Beijing.**

2.2 Single-particle soot photometer (SP2)

A single particle soot photometer (SP2, Droplet Measurement Technology, Inc., Boulder, CO, USA) was used to determine
655 the size distribution and mixing state of rBC particles in the atmosphere. In the SP2 measuring chamber, an intensive continuous intracavity Nd:YAG laser beam is generated (1064 nm, TEM00 mode). After an rBC-containing particle crosses

the beam, it is heated to incandescence by sequentially absorbing the laser power. The maximum incandescence intensity (or the peak height of the incandescence signal) is approximately linearly correlated with rBC's mass, irrespective of the presence of non-BC material or the rBC's morphology. The SP2 was calibrated to determine the relationship between the incandescence peak height and the mass of rBC particles using Aquadag aerosols (Acheson Inc., USA). Fig. 2b illustrates the schematic diagram of the calibration system. During calibration, monodisperse Aquadag aerosols were generated with an atomizer (model 3072, TSI Inc., USA) and dried using a diffusion dryer. Then, Aquadag aerosols with known mass (M_{rBC}) were selected with a CPMA and injected into the SP2 to obtain the corresponding laser-induced incandescence (LII) signal. A recent study (Laborde et al., 2012) demonstrated that the mass of rBC particles could be underestimated when using Aquadag aerosol as the calibration material. We performed a correction by multiplying by a factor of 0.75 for LII peak height during the calibration, as described in (Zhang et al., 2018; Liu et al., 2014). The LII peak- M_{rBC} relationship was thus obtained (Fig. S1). The uncertainty of the derived rBC mass was estimated to be 20%, which corresponds to an uncertainty of ~6% of the mass equivalent size (D_c , $D_c = \sqrt[3]{\frac{6* M_{rBC}}{\pi * \rho_{rBC}}}$) by using a 1.8 g cm⁻³ density for rBC material density (Bond et al., 2013).

In addition to the incandescence channel, SP2 also has scattering channels to directly measure the scattering cross section (σ_{measured}) of every single particle. However, for rBC-containing particles, the particles will evaporate during the measurement since rBC can absorb the laser energy, which results in a decrease in the rBC-containing particles' sizes and thus a decrease in the σ_{measured} . The leading-edge only (LEO) fitting method was invented to obtain the scattering cross section of the initial rBC-containing particles before evaporation (Gao et al., 2007). With the σ_{measured} and D_c , the diameter (D_p) of the rBC-containing particle can be obtained using Mie theory with refractive indices of 2.26-1.26i for the rBC (Moteki et al., 2010) and 1.48-0i for the coatings (Taylor et al., 2015) by assuming a core-shell structure. Thus, the coating thickness of rBC can be directly determined by SP2, as denoted by the shell/core ratio (D_p/D_c). The D_p derivation method based on LEO fitting has been widely used (Taylor et al., 2015; Shiraiwa et al., 2008; Liu et al., 2014; Laborde et al., 2013), and (Liu et al., 2015) estimated that the core-shell assumption will cause <6% uncertainty in the derived D_p/D_c . The scattering signal of SP2 was calibrated using polystyrene latex spheres (PSL, Nanosphere Size Standards, Duke Scientific Corp., USA) with known sizes (203±3 nm: Lot #185856; 303±3 nm: Lot #189903; 400±3 nm: Lot #189904), as shown in Fig. S2. The calibration of the scattering channel and the incandescence channel was also conducted after the observation. The calibration coefficient varied little (<3%) and the YAG power (laser intensity index recorded by the SP2) fluctuated by 4.8±0.1, indicating the stable condition of the SP2 during the observation period.

The detection efficiency of the SP2 was determined by comparing the number concentrations of Aquadag as simultaneously measured by the SP2 and a condensation particle counter (CPC, model 3775, TSI Inc., USA). For large particles, the SP2 detection efficiency was approximately unity and decreased gradually for smaller rBC particles (Fig. S3). For rBC with $D_c < 70$ nm, the detection efficiency of the SP2 fell significantly below 60%. The mass concentrations of rBC may be underestimated because of the low detection efficiency of for smaller rBC particles. By extrapolating a lognormal function fit

to the observed mass distribution, we found that rBC particles outside the detection range caused an ~15% underestimation of the rBC mass concentration. To compensate, the mass concentration of rBC was corrected by dividing by a factor of 0.85
690 during the measurement.

In general, the SP2 can directly measure the mass of the rBC core (M_{rBC}) and thus the mass equivalent diameter (D_c). Additionally, the scattering cross section ($\sigma_{measured}$) can be directly obtained by the SP2, and the diameter of the rBC-containing particle (D_p) can be derived using Mie theory.

2.3 Experiment

695 Two kinds of measurements were conducted in this study: a regular single SP2 observation to provide the number/mass size distribution and coating thickness of the rBC-containing particles and a tandem CPMA/DMA-SP2 experiment to study the microphysical properties of the rBC-containing particles.

2.3.1 Single SP2 measurement

700 The regular single SP2 observations were conducted from May 30 to June 7 and June 9 to June 12. An aerosol sampling inlet was placed at 4 m above the ground. A PM_{2.5} cyclone (URG-2000-30ENS-1) was used to selectively measure particles with an aerodynamic diameter smaller than 2.5 μm because rBC particles are typically present in the submicron mode. The systematic configuration of the rBC measurements is presented in Fig. 2a. A supporting pump with a flow rate of 9.6 L/min was used to guarantee a total inlet flow rate of 10 L/min (the demanding flow rate of a PM_{2.5} cyclone) and to minimize particle loss in the tube. The residence time of the sampling flow was estimated to be ~17 s. Then, the sample air was dried by passing
705 through a Nafion dryer (MD-700-24S, TSI) at a flow rate of 0.4 lpm. The dried sample was measured with the SP2 and CPC.

2.3.2 Tandem CPMA/DMA-SP2 measurement

710 The tandem CPMA/DMA-SP2 experiments were conducted on June 8 and 13. June 8 is representative of a clean period, when the concentrations of PM_{2.5} and O₃ averaged 20 $\mu\text{g}/\text{m}^3$ and 60 ppbv, respectively. Beijing was mainly affected by a clean northern air mass on June 8 (Fig. S5). June 13 is representative of a polluted period when the hourly mass concentration of PM_{2.5} exceeded 110 $\mu\text{g}/\text{m}^3$; the air mass was from the southern polluted area of Beijing, where many heavy industries are located. Thus, the tandem CPMA/DMA-SP2 experiment was conducted on June 8 and 13 to study the detailed physical characteristics of rBC under different pollution conditions.

715 As shown in Fig. 2(a), the tandem system was similar to the regular single SP2 observation system. The difference is the neutralizer, and a DMA or CPMA were added in front of the SP2, as denoted by the orange dashed line. Specifically, in the DMA-SP2 system, particles were first selected by DMA to obtain particles with known mobility diameters (D_{mob}). Then, the monodispersed particles were injected into the SP2 to obtain the corresponding information. In practice, we set three D_{mob} setpoints ($D_{mob} = 200 \text{ nm}, 250 \text{ nm}, 300 \text{ nm}$). The duration of one setpoint is ~20 min, and we recorded data 2 min after we changed the setpoint to allow the system to stabilize. The purpose of the DMA-SP2 system is to obtain the effective density

of bare rBC. Bare rBC is defined as rBC with $D_p/D_c \approx 1$, and the effective density of bare rBC was calculated according to the
720 following equation:

$$\rho_{eff} = \frac{6M_{rBC}}{\pi D_{mob}^3} \quad (5)$$

In principle, the measured effective density is the same as the material density if the particle has an ideal spherical shape with
no void space. Thus, the effective density is an indicator of particle compactness, as it compares the effective density and the
725 material density. Several studies that include the coupling of DMA with APM or CPMA have been conducted to determine
the ρ_{eff} - D_{mob} relationship of Aquadag rBC samples in the laboratory (Moteki and Kondo, 2010; Gysel et al., 2011). The
relationship between the ρ_{eff} and D_{mob} of Aquadag is presented in Fig. S4. The ρ_{eff} obtained using the DMA-SP2 system in this
study agreed well with previous research.

In the CPMA-SP2 system, particles with known mass (M_p) selected by CPMA were injected into the SP2, and the M_p setpoints
were 1 fg, 2 fg, 5 fg and 10 fg. The duration of one setpoint was ~20 min, and we waited 2 min after we changed the setpoints
730 to record a measurement. The purpose of the CPMA-SP2 system is to obtain morphological information about rBC-containing
particles with different coating degrees. Using a tandem CPMA-SP2 system, the mass of an rBC-containing particle (M_p) and
of the rBC core (M_{rBC}) can be simultaneously obtained. The coating thickness can be represented by the mass ratio of the
coating to the rBC core ($M_R = (M_p - M_{rBC})/M_{rBC}$) without any assumptions. Knowing M_p and M_{rBC} , the scattering cross section
735 of rBC-containing particles can be calculated through Mie theory with refractive indices of 2.26-1.26i for the rBC and 1.48i
for the coatings by assuming a core-shell structure and a coating density of 1.5 g/cm³. The calculated scattering cross section
(σ_{model}) can be compared to the $\sigma_{measured}$ by SP2, which can reflect the morphological characteristic of rBC-containing particles;
this comparison will be further discussed in section 4.1.2.

3 Results

740 3.1 Concentrations of PM_{2.5}, rBC and pollutant gases

The temporal variations in the concentrations of PM_{2.5}, rBC and gaseous pollutants (O₃, NO₂) during the project are presented
in Fig. 3. The regular pollutant concentrations, including PM_{2.5} (1405-F, ThermoFisher Scientific), NO₂ (42c, ThermoFisher
745 Scientific) and O₃ (49i, ThermoFisher Scientific), were obtained from a state control air quality site (2.5 km from LAPC),
provided by the China National Environmental Monitoring Centre. The mass concentration of PM_{2.5} ranged between 5 and
120 µg/m³ on a daily basis during the observation period. The mixing ratios of both NO₂ and O₃ exhibited obvious opposite
diurnal variations. The maximum O₃ concentration appeared at 1400 LST on June 2 with a value of 145 ppbv, reflecting high
atmospheric oxidant levels and strong photochemistry during the observation period. The mass concentration of rBC was 1.21
± 0.73 µg/m³ on average, accounting for 3.5 ± 2.4% of PM_{2.5} on an hourly basis, which was comparable to the previous filter-

based measurement in Beijing, with an average fraction of 3.2% in the summer of 2010 (Zhang et al., 2013). The mass concentration of rBC also exhibited a clear diurnal variation, with a maximum at night and a minimum at noon.

During the period from June 1 to June 6, the meteorological conditions were characterized by low relative humidity (RH < 40%) and strong solar radiation and were favorable for ozone formation. The mixing ratio of ozone was relatively high from June 1 to 6. On June 7, a heavy rainfall event occurred, and most of the major pollutants decreased due to significant wet scavenging. The mass concentration of $PM_{2.5}$ decreased from 65 to 10 $\mu g/m^3$, and the mass concentration of rBC decreased from 2.63 to 0.2 $\mu g/m^3$ from 0300–0700 LST on June 7. The pollutant concentration remained at a low level from June 7 to 8. After June 9, the ambient RH increased to 80%. Under high humidity conditions, the mass concentration of $PM_{2.5}$ experienced steady growth, increasing from 10 to 120 $\mu g/m^3$ and staying at a high level from June 12 to 13. Thus, the tandem DMA/CPMA-SP2 observations were conducted separately on June 8 and June 13, which separately represented the different $PM_{2.5}$ pollution conditions.

3.2 Size distribution of rBC

The number and mass distribution as a function of the D_c are illustrated in Fig. 4. As presented, the mass median diameter (MMD) was 171.2 nm during the project. A brief summary of the SP2 observations in China is presented in Table 1. Most previous studies focused on the rBC characteristics in winter when a larger MMD (~200–230 nm) was obtained (Zhang et al., 2013; Wu et al., 2017; Wang et al., 2016; Huang et al., 2012; Gong et al., 2016) than in this study. A similar MMD (180 nm) was reported in urban Shenzhen during a summer observation period (Lan et al., 2013), and a higher MMD (210–222 nm) was reported in winter. Liu et al. (2014) also found a winter-high-summer-low trend for rBC sizes in London, with $D_c=149\pm22$ nm in winter and 120 ± 6 nm in summer. Laboratory studies have proven that MMD is highly dependent on combustion conditions (Pan et al., 2017) and material. Thus, MMD is a suitable indicator of the sources of rBC. Several studies have suggested that the MMD of rBC from biomass burning and coal is much larger than that from traffic emissions (Wang et al., 2016; Schwarz et al., 2008). Huang et al. (2012) found the MMD observed at rural sites to be much larger than that observed at urban sites because urban sites are primarily affected by rBC emitted from traffic sources and rural sites are more influenced by rBC from coal combustion. The seasonal trends in MMD may be partially explained by the different rBC sources in summer and winter. Fig. 5 provides the temporal variations in the mass size distribution of rBC during the entire investigation period. Most rBC particles were within the size range of 70–300 nm, with a clear diurnal pattern. The diurnal cycle reached a peak plateau between 0300–0700 LST and decreased gradually in the afternoon. The cycle was controlled by the combined effects of the development of planetary boundary layer (PBL) variation and on-road rBC emissions.

After the two rain events (June 4 and June 7), the MMD decreased significantly from 186 nm to 170 nm and from 183 nm to 159 nm, respectively, as shown in Fig. 3. Taylor et al. (2014) observed that the rBC core size distribution shifted to smaller sizes after a biomass burning plume passed through a precipitating cloud, attributing this shift to the preferential nucleation scavenging of larger rBC cores. By counting the MMD on non-rainy days and rainy days, Wang et al. (2018) also found that

the MMD decreased from 164 ± 21 nm to 145 ± 25 nm. The decrease in MMD after rain events can be explained by the preferential wet scavenging of the larger rBC-containing particles.

A pollutant rose plot of MMD versus wind speed and wind direction is presented in Fig. 6a. The MMD of rBC was ~ 160 nm at low wind speed conditions and exhibited a significant increase with increasing southeast wind speed. The maximum MMD exceeded 190 nm when the wind speed was greater than 10 m/s. Fig. 6b presents the correlation between wind speed and MMD. A southerly wind period was selected when the wind direction was $135\text{--}225^\circ$, and a northerly wind period was the time when the wind direction was $325\text{--}45^\circ$. The MMD exhibited little correlation with wind speed and varied little between the south and northerly wind periods when the wind speeds were less than 2 m/s, as local rBC emissions were predominant. An MMD of $150\text{--}160$ nm during low wind speed periods may be characteristic of the local sources. The MMD had a strong positive correlation with the wind speed during the southerly wind period ($r^2 = 0.93$), suggesting that the rBC from the south was larger, which may be the result of the different rBC sources in the southern polluted region. Since the air mass from the north is always clean, the local rBC emissions may be the main contributors to the total rBC concentration in the northerly wind period. Thus, the MMD may be more influenced by local emissions and show a weak correlation with the wind speed during northerly wind periods.

3.3 Temporal variation of D_p/D_c

The D_p/D_c for a given single rBC-containing particle was calculated using the LEO fitting method. Herein, rBC cores with $D_c = 180 \pm 10$ nm were selected because the low scattering signal of small rBC is easily influenced by signal noise (D_p/D_c indicates the D_p/D_c with $D_c = 180 \pm 10$ nm in the following discussion if not specified). The D_p/D_c variation during the investigation time is illustrated in Fig. 7. In general, D_p/D_c was 1.20 ± 0.05 on average during the investigation, which is consistent with observations (1.15) during the summer in Paris (Laborde et al., 2013). rBC sources and the aging process significantly influenced the D_p/D_c of rBC. The rBC from traffic is reported to be relatively uncoated (Liu et al., 2014), whereas the rBC emitted by biomass burning is found to be moderately coated, with a $D_p/D_c = 1.2\text{--}1.4$ (Pan et al., 2017). Moreover, D_p/D_c increases with the aging process, and a larger D_p/D_c (1.6) was found in an aged continental air mass (Shiraiwa et al., 2008). The relatively low D_p/D_c value further supports the argument that rBC was primarily emitted from on-road vehicles during the summer in Beijing.

The D_p/D_c distributions for the two episodes before the tandem CPMA/DMA-SP2 experiments are shown in Fig. 7. Episode 1 (June 7 2200 LST – June 8 1200 LST) occurred after a heavy rain period and is representative of clean conditions. Episode 2 (June 11 2300 LST – June 12 1200 LST) was characterized by the highest D_p/D_c value (1.4) and the highest $\text{PM}_{2.5}$ concentration value ($120 \mu\text{g}/\text{m}^3$) during the observation period. The D_p/D_c exhibited a unimodal distribution during episode 1 and a clear bimodal pattern during episode 2, as shown in the upper panel of Fig. 7. The peak of the unimodal distribution and the left peak of the bimodal pattern correspond to a D_p/D_c value of ~ 1.05 , and the right peak of the bimodal pattern corresponds to a D_p/D_c value of ~ 1.8 . The rBC-containing particles with $D_p/D_c = 1.05$ may be freshly emitted by the local traffic. Zhang et al. (2018) demonstrated that 63% of the rBC was estimated to be transported from outside of Beijing during previous pollution

815 events, and the rBC-containing particles from regional transportation were characterized by having more coating material. The rBC-containing particles with $D_p/D_c = 1.8$ in the right peak of the bimodal distribution may be the result of transportation from polluted regions.

3.4 Diurnal variation in D_p/D_c

820 The temporal variation in D_p/D_c exhibited a clear day-high and night-low pattern. Fig. 8 exhibits the diurnal trend of D_p/D_c . The mean D_p/D_c increased during the daytime, with a peak (1.2) at 1400 LST and a minimum (1.12) at 0600 LST. D_p/D_c was controlled by the competing effects of emissions and aging because freshly emitted thinly coated rBC tends to decrease D_p/D_c and the aging process tends to increase D_p/D_c . The increasing trend of D_p/D_c during the day could be explained by the prevailing aging process, whereas the decreasing trend at night can be explained by the prevailing emissions process, as the photochemical condensation aging during the day was much faster than the coagulation aging at night (Riemer et al., 2004; Chen et al., 825 2017). By measuring the D_p from 0600–1400 LST, the D_p growth rate was calculated to be 2.34 nm/h. A larger D_p growth rate was found in the period with a high O_x concentration, which may be favorable for the formation of coating material on rBC. The photochemical process and condensation aging have proven to be very efficient during the day. Using a smog chamber, (Peng et al., 2016) found that the D_p growth rate of rBC-containing particles could reach 26 nm/h in Beijing's urban area.

830 Although the photochemical process and condensation may rapidly increase the D_p , the difference between the present study and the smog chamber results indicated that the "apparent" D_p growth rate in the ambient measurement was relatively low given the continuous freshly emitted rBC in urban Beijing. Thus, the D_p/D_c was always at a low level, resulting in little light absorption enhancement during the summer.

835 4 Discussion

4.1 Morphological evolution of rBC-containing particles

4.1.1 Morphology of bare rBC

840 By coupling DMA and SP2, the mass and the mobility diameter of bare rBC ($D_p/D_c \approx 1$) can be obtained simultaneously, and therefore, the effective density (ρ_{eff}) can be calculated. The ρ_{eff} of the ambient bare rBC was measured on a clean day (June 8) and a polluted day (June 13). The ρ_{eff} of bare rBC at 200–300 nm ranged from 0.41–0.29 g/cm³, which was much smaller than the material density of rBC (1.8 g/cm³). This significant discrepancy indicates that bare rBC was in a fractal structure consistent with the previous research from electron microscopic images, which showed that bare rBC was in a fractal chain-like structure (Adachi and Buseck, 2013; Li et al., 2003; Wang et al., 2017). ρ_{eff} showed no evident difference between the pollution day and the clean day because the bare rBC particles were freshly emitted and only affected by local sources. A power law is always used to describe the fractal-like aggregates of particles: $M_p \propto D_{mob}^{D_{fm}}$ (Moteki and Kondo, 2010; Park et al., 2004), where D_{fm} is defined as the mass fractal dimension that is an indicator of particle compactness. The value of D_{fm} is 3 for ideal spherical

particles and less than 3 for fractal particles. Based on the equation for ρ_{eff} , the following relationship can be found: $\rho_{\text{eff}} \propto D_{\text{mob}}^{D_{\text{fm}}-3}$. Thus, a larger bare rBC had a smaller ρ_{eff} , which was consistent with the results in Fig. 9. A power function was used to fit the observed data. $\rho_{\text{eff}} \propto D_{\text{mob}}^{-0.65}$ and $\rho_{\text{eff}} \propto D_{\text{mob}}^{-0.6}$ were found separately on clean and polluted days, corresponding to the mass fractal dimensions of 2.35 and 2.4, respectively. These mass fractal dimensions from the summer in Beijing are similar to the observations ($D_{\text{fm}}=2.3$) from urban Tokyo (Moteki and Kondo, 2010) and the diesel exhaust measurement ($D_{\text{fm}}=2.35$) (Park et al., 2004), suggesting that the freshly emitted bare rBC particles originated primarily from traffic sources. Traffic may contribute a majority of the fresh rBC during both polluted and clean periods in the summer.

4.1.2 Morphology of rBC-containing particles with increasing coating thickness

The morphological characteristics of rBC-containing particles were investigated by comparing the σ_{measured} and σ_{model} using a CPMA-SP2 system first proposed by (Liu et al., 2017). The comparison of σ_{measured} and σ_{model} as a function of M_R for a particle mass of 10 fg is illustrated in Fig. 10a. $\sigma_{\text{measured}}/\sigma_{\text{model}} = 1$ implies that the scattering cross section measured by SP2 is the same as the model prediction under the assumption of a core-shell structure; thus, the rBC-containing particle was likely a core-shell structure. When the rBC was bare ($M_R \approx 0$), the rBC was in a fractal structure, as discussed in section 4.1.1. With increasing M_R , the $\sigma_{\text{measured}}/\sigma_{\text{model}}$ gradually decreased until $M_R=1.5$, indicating that the coating material may not be sufficient to encapsulate rBC and that the rBC-containing particles tended not to be away from a core-shell structure. Liu et al. (2017) showed that rBC-containing particles with $M_R<1.5$ primarily presented an external structure. When $1.5 < M_R < 6$, the $\sigma_{\text{measured}}/\sigma_{\text{model}}$ steadily increased, which implied that the shape of rBC-containing particles gradually transformed to become more compact, with a core-shell-like structure, in this stage. When $M_R>6$, the $\sigma_{\text{measured}}/\sigma_{\text{model}}$ was equal to 1, indicating that the rBC-containing particles were in a core-shell-like structure in this stage. Similar phenomena were found in the relationship of $\sigma_{\text{measured}}/\sigma_{\text{model}}$ and M_R for particle masses of 5 fg, as illustrated in Fig. 10b. However, when $M_R \approx 0.1$, the σ_{measured} was consistent with the model prediction for a particle mass of 5 fg. This is because the scattering signal was not sensitive to the irregularity of smaller-sized particles (Moteki et al., 2010). Therefore, a Mie theory-based core-shell model could capture the main morphological features.

Different techniques have been used to explore the morphology of rBC-containing particles in ambient and laboratory measurements (Zhang et al., 2008; Peng et al., 2016; Pagels et al., 2009). It is generally agreed that the morphology of rBC-containing particles will become more compact with the aging process or with increasing coating thickness. However, this study reveals that the morphology transform may only be true when the coating is thick enough ($M_R>1.5$), and the coatings may only attach to rBC and slightly influence rBC-containing particles' morphology when the coating is not thick enough ($M_R<1.5$).

Based on the relationship between the $\sigma_{\text{measured}}/\sigma_{\text{model}}$ and M_R , the rBC-containing particles are classified into three groups: external stage ($0 < M_R < 1.5$), transit stage ($1.5 < M_R < 6$) and core-shell stage ($M_R > 6$). A similar variation between the

880 $\sigma_{\text{measured}}/\sigma_{\text{model}}$ and M_R was also found by (Liu et al., 2017; Wu et al., 2018). The M_R transition point from the transit stage and core-shell stage determined by (Liu et al., 2017) is slightly lower than that in this study. Liu et al. (2017) found that the M_R transition point varied among different rBC sources. In addition to rBC sources, the environmental conditions during the aging process of rBC-containing particles, such as temperature and humidity, may also influence the rBC-containing particle morphology. We determined the M_R transition point in Beijing in summer. More work needs to be done in the future to better quantify M_R in different situations.

885 The combined CPMA and SP2 measurements were conducted separately on a clean day (June 8) and a polluted day (June 13). Fig. 11(a) presents the average M_R for different CPMA setpoints (1 fg, 2 fg, 5 fg, and 10 fg) on June 8 and June 13. The average M_R is 0.77 for $M_p=1$ fg and 5.29 for $M_p=10$ fg on the clean day, whereas the average M_R is 0.84 for $M_p=1$ fg and 7.28 for $M_p=10$ fg on the pollution day. The average M_R values of the polluted day were all larger than those on the clean day for the four M_p points. This result demonstrated that rBC had more coating material on the polluted day than on the clean day. Based on 890 the M_R transition points discussed above, the rBC-containing particles were classified into three stages as shown in Fig. 11(b). The rBC-containing particles with $M_p=1$ fg were primarily in the external mixing stage regardless of the pollution conditions. With an increase in M_p , more rBC-containing particles were in the transition or core-shell stage. On the clean day, 28% of the rBC-containing particles were in the core-shell stage, when $M_p=10$ fg. However, on the pollution day, 45% of the rBC-containing particles were in the core-shell stage, when $M_p=10$ fg. This phenomenon implied that most rBC-containing particles 895 are not in an ideal core-shell structure on clean days, whereas more rBC-containing particles were in a core-shell structure with thicker coatings on the pollution day.

4.2 Implications of rBC-containing particle morphology for light absorption

900 The morphology of rBC-containing particles varied with M_R . A simple core-shell model, as always used in the previous research to determine optical properties, will certainly cause bias. Based on the classification of the rBC-containing particles according to the relationship between $\sigma_{\text{measured}}/\sigma_{\text{model}}$ and M_R , Liu et al. (2017) proposed a simple morphology-dependent scheme in which the rBC-containing particles at the external stage were considered to have no absorption enhancement (E_{abs}) and the rBC-containing particles at the core-shell stage were considered to have the same E_{abs} from Mie theory under the assumption of a perfect core-shell structure. The E_{abs} at the transit stage was calculated by the interpolation of E_{abs} between the external and core-shell stages. A graphical and detailed description of the calculation of E_{abs} can be found in Fig. S6. Liu et al. 905 (2017) proved that this morphology-dependent scheme is in good agreement with the measured E_{abs} . Thus, the E_{abs} at 550 nm wavelength with $D_c=180\pm10$ nm was calculated separately using the core-shell model and the morphology-dependent scheme to quantify the uncertainty of using a core-shell model, as shown in Fig. 12. E_{abs} was 1.15, on average, using the core-shell model but was only 1.03 using the new scheme. The E_{abs} determined by the core-shell model was overestimated 11.7% because the observed averaged coating thickness ($D_p/D_c=1.2$) determined from single SP2 measurements corresponded to $M_R=0.37$, 910 suggesting that the coating material was not sufficient and most of the rBC-containing particles were not in a core-shell

structure in summer in Beijing. Thus, it is necessary to consider the morphology of rBC-containing particles when calculating their optical properties.

5 Conclusion

The mixing characteristics of rBC-containing particles were investigated in Beijing during the early summer of 2018 using a single particle soot photometer (SP2). The rBC had an approximately log-normal distribution as a function of the mass equivalent diameter (D_c), characterized by a mass median diameter (MMD) of 171.2 nm, which is consistent with previous urban measurements. The mass size distribution was highly associated with the meteorological conditions. Heavy rain events caused the rBC mass size distribution to be smaller, indicating that wet scavenging may be a more efficient removal mechanism for larger rBC-containing particles. The mass size distribution of rBC shifted to larger sizes when southerly winds prevailed, which was primarily caused by the different rBC sources in the south.

The D_p/D_c was 1.20 on average, with $D_c=180$ nm during the investigation period, indicating a low coating thickness of rBC during the summer. D_p/D_c exhibited a clear diurnal pattern with a peak at 1400 LST, increasing from 0600 to 1400 LST at a D_p growth rate of 2.34 nm/h, with $D_c=180$ nm during the day. The growth rate was much higher in high O_x periods. However, this growth rate was significantly lower than that in the smog chamber results, with a growth rate of 26 nm/h, because the continuously emitted fresh rBC lowered the D_p/D_c in ambient measurements. Although photochemical aging may be very efficient, with continuously emitted fresh rBC, the D_p/D_c increase in the ambient air was very slow, indicating that the rBC-containing particles were primarily at a low D_p/D_c level in summer.

A tandem measurement system with a differential mobility analyzer (DMA) and a centrifugal particle mass analyzer (CPMA) were coupled with an SP2 to investigate the detailed characteristics of rBC-containing particles in summer. The results showed that the effective density of bare rBC ($D_p/D_c=1$) was determined to be 0.41–0.30 g/cm³ for $D_c=200$ –300 nm. These effective densities were significantly lower than the rBC material density (1.8 g/cm³), suggesting that the bare rBC was in a fractal structure. The corresponding mass fractal dimension (D_{fm}) was 2.35, which agrees well with the D_{fm} of the direct measurement from vehicles, and was unchanged regardless of pollution, indicating that traffic emissions are a major source of fresh bare rBC on both clean and polluted days during the summer in Beijing. With increasing coating thickness, the morphology of rBC changed from a fractal structure to a compact core-shell structure. When M_R (M_{coat}/M_{rBC}) < 1.5, rBC-containing particles were in an external structure. When $M_R > 6$, rBC-containing particles were in a core-shell structure. When $1.5 < M_R < 6$, the rBC-containing particles were in a transition stage.

Based on the core-shell model and Mie theory, a new morphology-dependent absorption enhancement (E_{abs}) scheme was proposed and applied to the ambient measurements. A simulation showed that the E_{abs} averaged 1.03 with $D_c=180$ nm at a wavelength of 550 nm in the summer. The core-shell model overestimated the E_{abs} by 11.7%.

Data availability

To request the data given in this study, please contact Dr. Xiaole Pan at the Institute of Atmospheric Physics, Chinese Academy of Sciences, via email (panxiaole@mail.iap.ac.cn).

Author contributions

945 H. L and X. P designed the research; H. L, X. P, X. L, Y. T, Y. S, P. F, and Z. W performed the experiments; H. L, X. P, D. L, and X. C performed the data analysis; H. L and X. P wrote the paper.

Competing interests

The authors declare that they have no conflict of interest.

Acknowledgements

950 This study was supported by the National Natural Science Foundation of China (grant No. 41877314, 41675128).

Reference

Adachi, K., and Buseck, P. R.: Changes of ns-soot mixing states and shapes in an urban area during CalNex, *J. Geophys. Res.-Atmos.*, 118, 3723-3730, 10.1002/jgrd.50321, 2013.

955 Adler, G., Riziq, A. A., Erlick, C., and Rudich, Y.: Effect of intrinsic organic carbon on the optical properties of fresh diesel soot, *P Natl Acad Sci USA*, 107, 6699-6704, 10.1073/pnas.0903311106, 2010.

Apte, J. S., Marshall, J. D., Cohen, A. J., and Brauer, M.: Addressing Global Mortality from Ambient PM2.5, *Environ Sci Technol*, 49, 8057-8066, 10.1021/acs.est.5b01236, 2015.

960 Bond, T. C., Doherty, S. J., Fahey, D., Forster, P., Berntsen, T., DeAngelo, B., Flanner, M., Ghan, S., Kärcher, B., and Koch, D.: Bounding the role of black carbon in the climate system: A scientific assessment, *Journal of Geophysical Research: Atmospheres*, 118, 5380-5552, 2013.

Bond, T. C., Doherty, S. J., Fahey, D., Forster, P., Berntsen, T., DeAngelo, B., Flanner, M., Ghan, S., Kärcher, B., and Koch, D.: Bounding the role of black carbon in the climate system: A scientific assessment, *Journal of Geophysical Research: Atmospheres*, 118, 5380-5552, 2013.

965 Cao, J. J., Lee, S. C., Ho, K. F., Zou, S. C., Fung, K., Li, Y., Watson, J. G., and Chow, J. C.: Spatial and seasonal variations of atmospheric organic carbon and elemental carbon in Pearl River Delta Region, China, *Atmos Environ*, 38, 4447-4456, 10.1016/j.atmosenv.2004.05.016, 2004.

Cao, J. J., Lee, S. C., Chow, J. C., Watson, J. G., Ho, K. F., Zhang, R. J., Jin, Z. D., Shen, Z. X., Chen, G. C., Kang, Y. M., Zou, S. C., Zhang, L. Z., Qi, S. H., Dai, M. H., Cheng, Y., and Hu, K.: Spatial and seasonal distributions of carbonaceous aerosols over China, *J. Geophys. Res.-Atmos.*, 112, Artn D22s1110.1029/2006jd008205, 2007.

970 Cappa, C. D., Onasch, T. B., Massoli, P., Worsnop, D. R., Bates, T. S., Cross, E. S., Davidovits, P., Hakala, J., Hayden, K. L., Jobson, B. T., Kolesar, K. R., Lack, D. A., Lerner, B. M., Li, S. M., Mellon, D., Nuaaman, I., Olfert, J. S., Petaja, T., Quinn, P. K., Song, C., Subramanian, R., Williams, E. J., and Zaveri, R. A.: Radiative Absorption Enhancements Due to the Mixing State of Atmospheric Black Carbon, *Science*, 337, 1078-1081, 10.1126/science.1223447, 2012.

Chen, X. S., Wang, Z. F., Yu, F. Q., Pan, X. L., Li, J., Ge, B. Z., Wang, Z., Hu, M., Yang, W. Y., and Chen, H. S.: Estimation of atmospheric aging time of black carbon particles in the polluted atmosphere over central-eastern China using microphysical process analysis in regional chemical transport model, *Atmos Environ*, 163, 44-56, 10.1016/j.atmosenv.2017.05.016, 2017.

975 Cheng, Y. F., Su, H., Rose, D., Gunthe, S. S., Berghof, M., Wehner, B., Achtert, P., Nowak, A., Takegawa, N., Kondo, Y., Shiraiwa, M., Gong, Y. G., Shao, M., Hu, M., Zhu, T., Zhang, Y. H., Carmichael, G. R., Wiedensohler, A., Andreae, M. O., and Poschl, U.: Size-resolved measurement of the mixing state of soot in the megacity Beijing, China: diurnal cycle, aging and parameterization, *Atmospheric Chemistry and Physics*, 12, 4477-4491, 10.5194/acp-12-4477-2012, 2012.

980 Ding, A. J., Huang, X., Nie, W., Sun, J. N., Kerminen, V. M., Petaja, T., Su, H., Cheng, Y. F., Yang, X. Q., Wang, M. H., Chi, X. G., Wang, J. P., Virkkula, A., Guo, W. D., Yuan, J., Wang, S. Y., Zhang, R. J., Wu, Y. F., Song, Y., Zhu, T., Zilitinkevich, S., Kulmala, M., and Fu, C. B.: Enhanced haze pollution by black carbon in megacities in China, *Geophysical Research Letters*, 43, 2873-2879, 10.1002/2016gl067745, 2016.

985 Gao, R. S., Schwarz, J. P., Kelly, K. K., Fahey, D. W., Watts, L. A., Thompson, T. L., Spackman, J. R., Slowik, J. G., Cross, E. S., Han, J. H., Davidovits, P., Onasch, T. B., and Worsnop, D. R.: A novel method for estimating light-scattering properties of soot aerosols using a modified single-particle soot photometer, *Aerosol Science and Technology*, 41, 125-135, 10.1080/02786820601118398, 2007.

Gong, X. D., Zhang, C., Chen, H., Nizkorodov, S. A., Chen, J. M., and Yang, X.: Size distribution and mixing state of black carbon particles during a heavy air pollution episode in Shanghai, *Atmospheric Chemistry and Physics*, 16, 5399-5411, 10.5194/acp-16-5399-2016, 2016.

990 Gysel, M., Laborde, M., Olfert, J. S., Subramanian, R., and Grohn, A. J.: Effective density of Aquadag and fullerene soot black carbon reference materials used for SP2 calibration, *Atmos Meas Tech*, 4, 2851-2858, 10.5194/amt-4-2851-2011, 2011.

Huang, X. F., Sun, T. L., Zeng, L. W., Yu, G. H., and Luan, S. J.: Black carbon aerosol characterization in a coastal city in South China using a single particle soot photometer, *Atmos Environ*, 51, 21-28, 10.1016/j.atmosenv.2012.01.056, 2012.

995 Jacobson, M. Z.: Strong radiative heating due to the mixing state of black carbon in atmospheric aerosols, *Nature*, 409, 695-697, Doi 10.1038/35055518, 2001.

Laborde, M., Mertes, P., Zieger, P., Dommen, J., Baltensperger, U., and Gysel, M.: Sensitivity of the Single Particle Soot Photometer to different black carbon types, *Atmos Meas Tech*, 5, 1031-1043, 10.5194/amt-5-1031-2012, 2012.

1000 Laborde, M., Crippa, M., Tritscher, T., Juranyi, Z., Decarlo, P. F., Temime-Roussel, B., Marchand, N., Eckhardt, S., Stohl, A., Baltensperger, U., Prevot, A. S. H., Weingartner, E., and Gysel, M.: Black carbon physical properties and mixing state in the European megacity Paris, *Atmospheric Chemistry and Physics*, 13, 5831-5856, 10.5194/acp-13-5831-2013, 2013.

Lack, D. A., Langridge, J. M., Bahreini, R., Cappa, C. D., Middlebrook, A. M., and Schwarz, J. P.: Brown carbon and internal mixing in biomass burning particles, *P Natl Acad Sci USA*, 109, 14802-14807, 10.1073/pnas.1206575109, 2012.

1005 Lan, Z. J., Huang, X. F., Yu, K. Y., Sun, T. L., Zeng, L. W., and Hu, M.: Light absorption of black carbon aerosol and its enhancement by mixing state in an urban atmosphere in South China, *Atmos Environ*, 69, 118-123, 10.1016/j.atmosenv.2012.12.009, 2013.

Li, J., Posfai, M., Hobbs, P. V., and Buseck, P. R.: Individual aerosol particles from biomass burning in southern Africa: 2, Compositions and aging of inorganic particles, *J. Geophys. Res.-Atmos.*, 108, 2003.

1010 Liu, D., Allan, J., Whitehead, J., Young, D., Flynn, M., Coe, H., McFiggans, G., Fleming, Z. L., and Bandy, B.: Ambient black carbon particle hygroscopic properties controlled by mixing state and composition, *Atmospheric Chemistry and Physics*, 13, 2015-2029, 10.5194/acp-13-2015-2013, 2013.

Liu, D., Allan, J. D., Young, D. E., Coe, H., Beddows, D., Fleming, Z. L., Flynn, M. J., Gallagher, M. W., Harrison, R. M., Lee, J., Prevot, A. S. H., Taylor, J. W., Yin, J., Williams, P. I., and Zotter, P.: Size distribution, mixing state and source apportionment of black carbon aerosol in London during wintertime, *Atmospheric Chemistry and Physics*, 14, 10061-10084, 10.5194/acp-14-10061-2014, 2014.

1015 Liu, D. T., Taylor, J. W., Young, D. E., Flynn, M. J., Coe, H., and Allan, J. D.: The effect of complex black carbon microphysics on the determination of the optical properties of brown carbon, *Geophysical Research Letters*, 42, 613-619, 10.1002/2014gl062443, 2015.

Liu, D. T., Whitehead, J., Alfarra, M. R., Reyes-Villegas, E., Spracklen, D. V., Reddington, C. L., Kong, S. F., Williams, P. I., Ting, Y. C., Haslett, S., Taylor, J. W., Flynn, M. J., Morgan, W. T., McFiggans, G., Coe, H., and Allan, J. D.: Black-carbon absorption enhancement in the atmosphere determined by particle mixing state, *Nat Geosci*, 10, 184-U132, 10.1038/Ngeo2901, 2017.

Menon, S., Hansen, J., Nazarenko, L., and Luo, Y.: Climate effects of black carbon aerosols in China and India, *Science*, 297, 2250-2253, 2002.

Moteki, N., and Kondo, Y.: Dependence of Laser-Induced Incandescence on Physical Properties of Black Carbon Aerosols:

1025 Measurements and Theoretical Interpretation, *Aerosol Science and Technology*, 44, 663-675, Pii 924375405
10.1080/02786826.2010.484450, 2010.

Moteki, N., Kondo, Y., and Nakamura, S.: Method to measure refractive indices of small nonspherical particles: Application to black carbon particles, *J Aerosol Sci*, 41, 513-521, 10.1016/j.jaerosci.2010.02.013, 2010.

1030 Pagels, J., Khalizov, A. F., McMurry, P. H., and Zhang, R. Y.: Processing of Soot by Controlled Sulphuric Acid and Water Condensation Mass and Mobility Relationship, *Aerosol Science and Technology*, 43, 629-640, Pii 910341827
10.1080/02786820902810685, 2009.

Pan, X. L., Kanaya, Y., Taketani, F., Miyakawa, T., Inomata, S., Komazaki, Y., Tanimoto, H., Wang, Z., Uno, I., and Wang, Z. F.: Emission characteristics of refractory black carbon aerosols from fresh biomass burning: a perspective from laboratory experiments, *Atmospheric Chemistry and Physics*, 17, 13001-13016, 10.5194/acp-17-13001-2017, 2017.

1035 Park, K., Kittelson, D. B., and McMurry, P. H.: Structural properties of diesel exhaust particles measured by transmission electron microscopy (TEM): Relationships to particle mass and mobility, *Aerosol Science and Technology*, 38, 881-889, 10.1080/027868290505189, 2004.

Peng, J. F., Hu, M., Guo, S., Du, Z. F., Zheng, J., Shang, D. J., Zamora, M. L., Zeng, L. M., Shao, M., Wu, Y. S., Zheng, J., Wang, Y., Glen, C. R., Collins, D. R., Molina, M. J., and Zhang, R. Y.: Markedly enhanced absorption and direct radiative forcing of black carbon under polluted urban environments, *P Natl Acad Sci USA*, 113, 4266-4271, 10.1073/pnas.1602310113, 2016.

1040 Popovicheva, O. B., Persantseva, N. M., Kireeva, E. D., Khokhlova, T. D., and Shonija, N. K.: Quantification of the Hygroscopic Effect of Soot Aging in the Atmosphere: Laboratory Simulations, *J Phys Chem A*, 115, 298-306, 10.1021/jp109238x, 2011.

1045 Qin, Y., and Xie, S. D.: Spatial and temporal variation of anthropogenic black carbon emissions in China for the period 1980-2009, *Atmospheric Chemistry and Physics*, 12, 4825-4841, 10.5194/acp-12-4825-2012, 2012.

Ramanathan, V., Crutzen, P. J., Kiehl, J. T., and Rosenfeld, D.: Atmosphere - Aerosols, climate, and the hydrological cycle, *Science*, 294, 2119-2124, DOI 10.1126/science.1064034, 2001.

1050 Ramanathan, V., and Carmichael, G.: Global and regional climate changes due to black carbon, *Nat Geosci*, 36, págs. 335-358, 2008.

Riemer, N., Vogel, H., and Vogel, B.: Soot aging time scales in polluted regions during day and night, *Atmospheric Chemistry and Physics*, 4, 1885-1893, DOI 10.5194/acp-4-1885-2004, 2004.

1055 Schnaiter, M., Linke, C., Möhler, O., Naumann, K. H., Saathoff, H., Wagner, R., Schurath, U., and Wehner, B.: Absorption amplification of black carbon internally mixed with secondary organic aerosol, *Journal of Geophysical Research Atmospheres*, 110, -, 2005.

Schwarz, J. P., Gao, R. S., Spackman, J. R., Watts, L. A., Thomson, D. S., Fahey, D. W., Ryerson, T. B., Peischl, J., Holloway, J. S., Trainer, M., Frost, G. J., Baynard, T., Lack, D. A., de Gouw, J. A., Warneke, C., and Del Negro, L. A.: Measurement of the mixing state, mass, and optical size of individual black carbon particles in urban and biomass burning emissions, *Geophysical Research Letters*, 35, Artn L1381010.1029/2008gl033968, 2008.

1060 Shiraiwa, M., Kondo, Y., Moteki, N., Takegawa, N., Sahu, L., Takami, A., Hatakeyama, S., Yonemura, S., and Blake, D.: Radiative impact of mixing state of black carbon aerosol in Asian outflow, *Journal of Geophysical Research: Atmospheres*, 113, 2008.

Shiraiwa, M., Kondo, Y., Iwamoto, T., and Kita, K.: Amplification of Light Absorption of Black Carbon by Organic Coating, *Aerosol Science and Technology*, 44, 46-54, 10.1080/02786820903357686, 2010.

1065 Taylor, J. W., Allan, J. D., Allen, G., Coe, H., Williams, P. I., Flynn, M. J., Le Breton, M., Muller, J. B. A., Percival, C. J., Oram, D., Forster, G., Lee, J. D., Rickard, A. R., Parrington, M., and Palmer, P. I.: Size-dependent wet removal of black carbon in Canadian biomass burning plumes, *Atmospheric Chemistry and Physics*, 14, 13755-13771, 10.5194/acp-14-13755-2014, 2014.

Taylor, J. W., Allan, J. D., Liu, D., Flynn, M., Weber, R., Zhang, X., Lefer, B. L., Grossberg, N., Flynn, J., and Coe, H.: 1070 Assessment of the sensitivity of core/shell parameters derived using the single-particle soot photometer to density and refractive index, *Atmos Meas Tech*, 8, 1701-1718, 10.5194/amt-8-1701-2015, 2015.

Wang, Q. Y., Huang, R. J., Zhao, Z. Z., Cao, J. J., Ni, H. Y., Tie, X. X., Zhao, S. Y., Su, X. L., Han, Y. M., Shen, Z. X., Wang, Y. C., Zhang, N. N., Zhou, Y. Q., and Corbin, J. C.: Physicochemical characteristics of black carbon aerosol and its radiative impact in a polluted urban area of China, *J. Geophys. Res.-Atmos.*, 121, 12505-12519, 10.1002/2016jd024748, 2016.

1075 Wang, Q. Y., Cao, J. J., Han, Y. M., Tian, J., Zhu, C. S., Zhang, Y. G., Zhang, N. N., Shen, Z. X., Ni, H. Y., Zhao, S. Y., and Wu, J. R.: Sources and physicochemical characteristics of black carbon aerosol from the southeastern Tibetan Plateau: internal mixing enhances light absorption, *Atmospheric Chemistry and Physics*, 18, 4639-4656, 10.5194/acp-18-4639-2018, 2018.

1080 Wang, Y. Y., Liu, F. S., He, C. L., Bi, L., Cheng, T. H., Wang, Z. L., Zhang, H., Zhang, X. Y., Shi, Z. B., and Li, W. J.: Fractal Dimensions and Mixing Structures of Soot Particles during Atmospheric Processing, *Environ Sci Tech Let*, 4, 487-493, 10.1021/acs.estlett.7b00418, 2017.

1085 Wu, Y., Cheng, T. H., Liu, D. T., Allan, J. D., Zheng, L. J., and Chen, H.: Light Absorption Enhancement of Black Carbon Aerosol Constrained by Particle Morphology, *Environ Sci Technol*, 52, 6912-6919, 10.1021/acs.est.8b00636, 2018.

1090 Wu, Y. F., Wang, X. J., Tao, J., Huang, R. J., Tian, P., Cao, J. J., Zhang, L. M., Ho, K. F., Han, Z. W., and Zhang, R. J.: Size distribution and source of black carbon aerosol in urban Beijing during winter haze episodes, *Atmospheric Chemistry and Physics*, 17, 7965-7975, 10.5194/acp-17-7965-2017, 2017.

1095 Zhang, R., Jing, J., Tao, J., Hsu, S. C., Wang, G., Cao, J., Lee, C. S. L., Zhu, L., Chen, Z., Zhao, Y., and Shen, Z.: Chemical characterization and source apportionment of PM2.5 in Beijing: seasonal perspective, *Atmospheric Chemistry and Physics*, 13, 7053-7074, 10.5194/acp-13-7053-2013, 2013.

Zhang, R. J., Ho, K. F., Cao, J. J., Han, Z. W., Zhang, M. G., Cheng, Y., and Lee, S. C.: Organic carbon and elemental carbon associated with PM10 in Beijing during spring time, *J Hazard Mater*, 172, 970-977, 10.1016/j.jhazmat.2009.07.087, 2009.

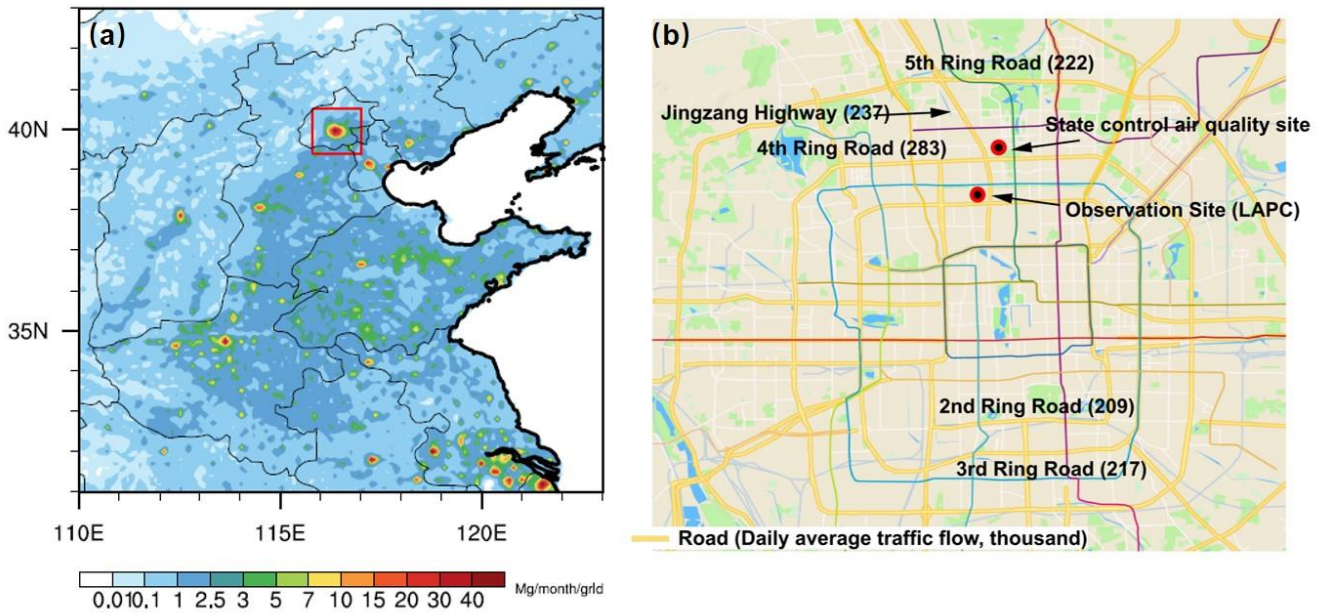
Zhang, R. Y., Khalizov, A. F., Pagels, J., Zhang, D., Xue, H. X., and McMurry, P. H.: Variability in morphology, hygroscopicity, and optical properties of soot aerosols during atmospheric processing, *P Natl Acad Sci USA*, 105, 10291-10296, 10.1073/pnas.0804860105, 2008.

Zhang, Y. X., Zhang, Q., Cheng, Y. F., Su, H., Li, H. Y., Li, M., Zhang, X., Ding, A. J., and He, K. B.: Amplification of light absorption of black carbon associated with air pollution, *Atmospheric Chemistry and Physics*, 18, 9879-9896, 10.5194/acp-18-9879-2018, 2018.

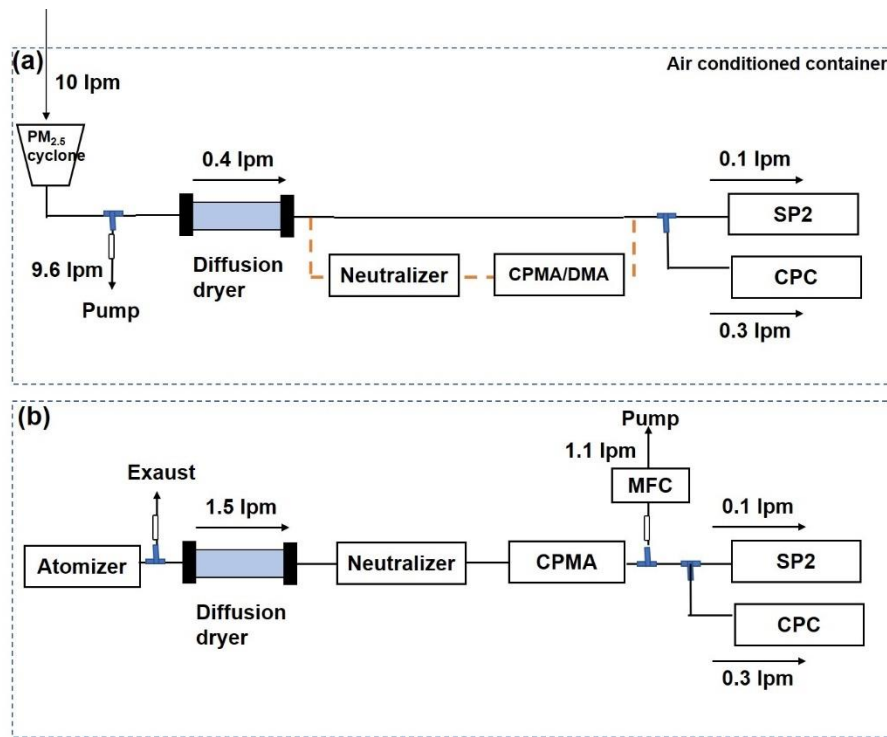
1100 **Table 1.** Brief summary of some of the observations on the mixing state of rBC-containing particles.

rBC type	Site	Period	MMD (nm)	D_p/D_c	Description	Reference
Urban emissions (UE)	Shenzhen, China	Aug–Sep (summer)	180*		The measurement station was on a university campus located in the urban area of Shenzhen.	(Lan et al., 2013)
	Shenzhen, China	Jan–Feb (winter)	210*		The measurement station was the same as the above site.	(Huang et al., 2012)
	Shanghai, China	Dec (winter)	200	2–8	The maximum PM _{2.5} mass loading reached 636 $\mu\text{g}/\text{m}^3$.	(Gong et al., 2016)
	Beijing, China	Feb–Mar (winter)	213		The same measurement site as this study.	(Wu et al., 2017)
This study		Jun (summer)	171	1.2 ($D_c=180 \text{ nm}$)		
London, United Kingdom		Jan–Feb (winter)	149	1.2–2 ($D_c=110–150 \text{ nm}$)	During the Clean Air for London (ClearfLo) project.	(Liu et al., 2014)
		Jul–Aug (summer)	120			
Biomass burning (BB)	Airborne measurements	Sep (autumn)	210	1.33 ($D_c=190–210 \text{ nm}$)	The MMD and D_p/D_c were both higher for BB than UE.	(Schwarz et al., 2008)
			189	1.2–1.4 ($D_c=200 \text{ nm}$)	Fresh, laboratory-produced biomass burning rBC.	(Pan et al., 2017)
	Airborne measurements	Jul–Aug (summer)	195	2.35 ($D_c=130–230 \text{ nm}$)	During the second phase of the BORTAS project.	(Taylor et al., 2014)

* Assuming the density of rBC is 2 g/cm³



1105
Figure 1. (a) Monthly emissions of BC from traffic in June in east-central China. The red box denotes the geographical location of the observation site, the map is the built-in map of the NCL software (<http://www.ncl.ucar.edu/>). (b) Road map and traffic flow rate of Beijing. The red circle denotes the observation site.



1110
Figure 2. Schematic diagram of (a) the measurement system, with the orange dashed line denoting the tandem CPMA/DMA-SP2 measurement system, during the periods June 9 and 13, and (b) the calibration system.

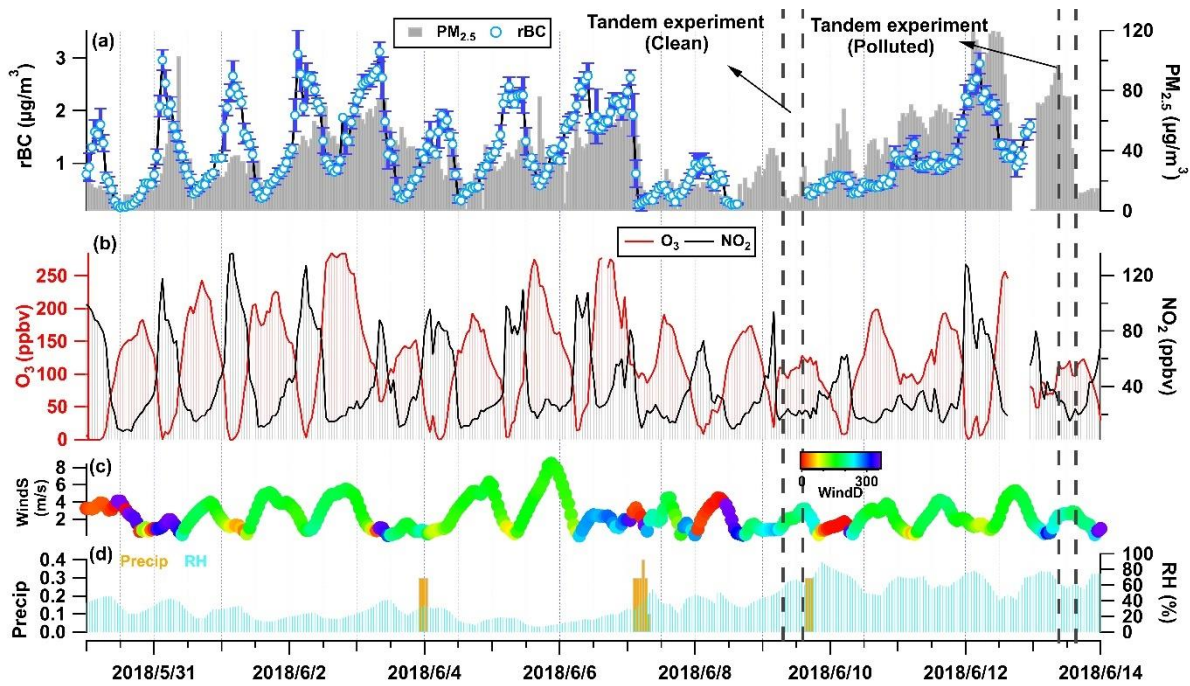


Figure 3. Time series of aerosol/gaseous pollutants and meteorological conditions during the observation period.

1115

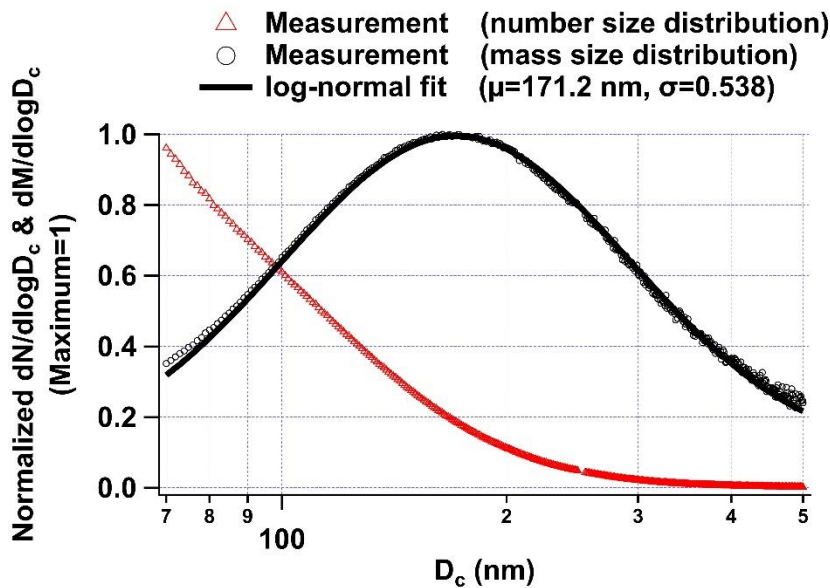
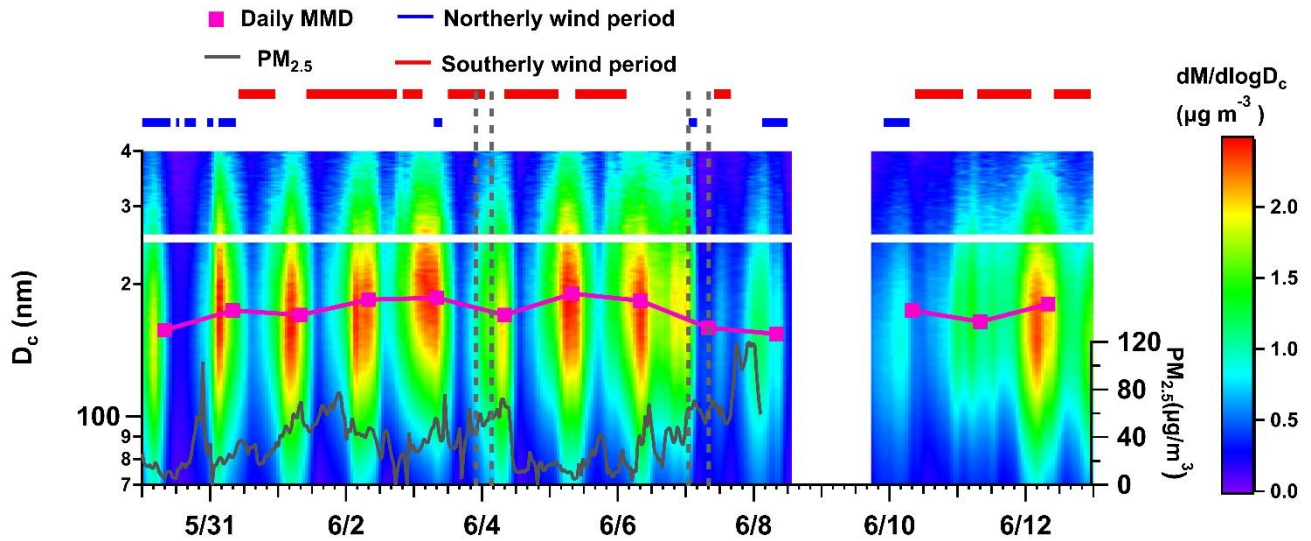
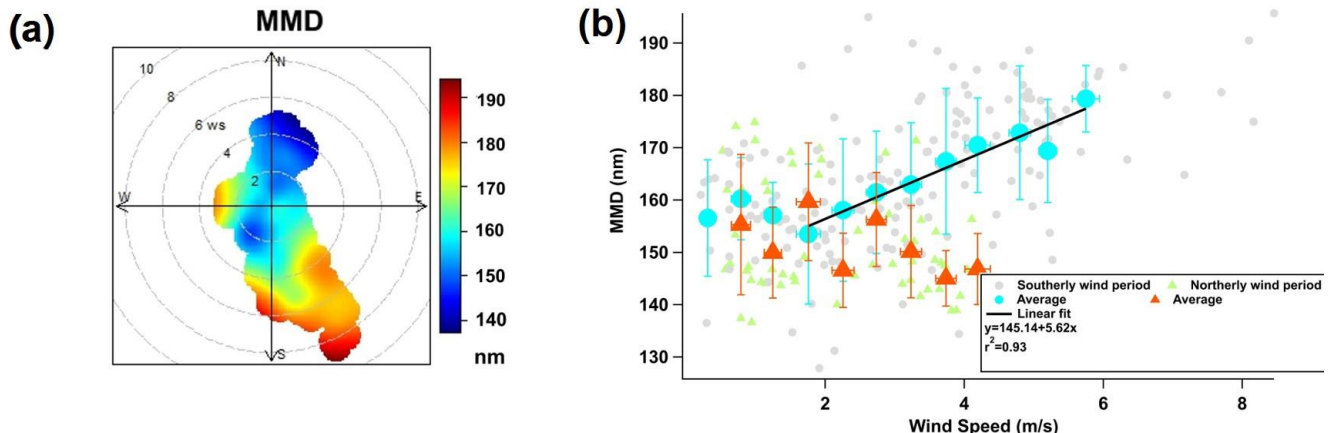


Figure 4. Number and mass size distribution ($dN/d\log D_c$ & $dM/d\log D_c$) during the observation period.



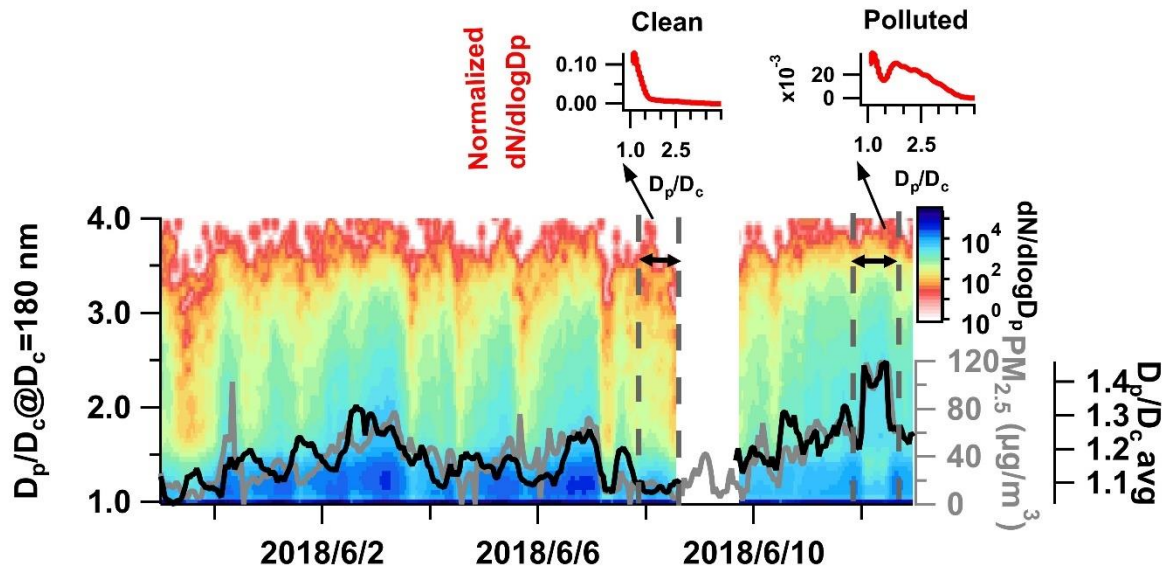
1120

Figure 5. Time series of the mass size distribution of rBC. A southerly wind period is selected when the wind direction is 135–225° and a northerly wind period is the time when the wind direction is 325–45°. The gray dashed line denotes the rainy period.



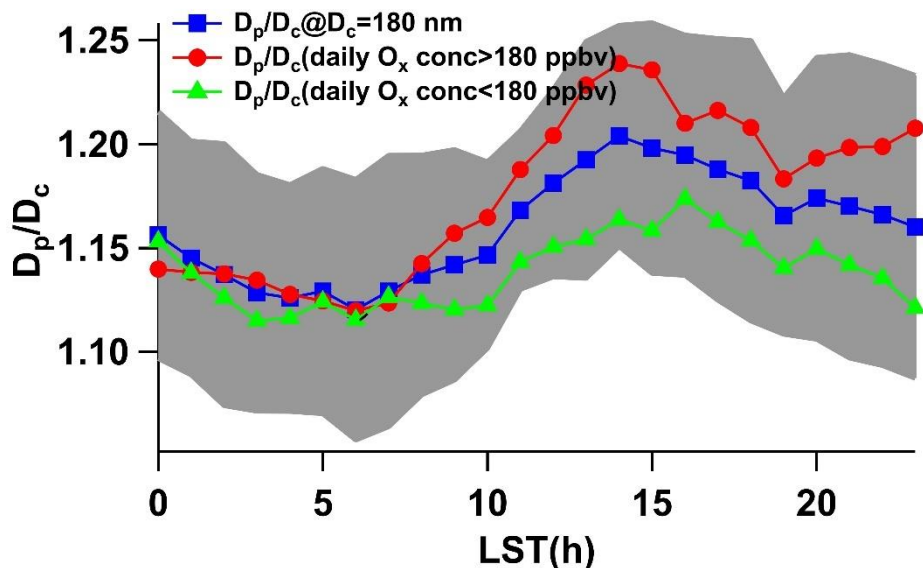
1125

Figure 6. (a) Dependence of rBC's MMD on wind speed and wind direction during the observation period. (b) MMD versus wind speed during the southerly wind period and northerly wind period. The error bars correspond to the standard deviations of MMD in each wind speed bin.



1130

Figure 7. Temporal variation in D_p/D_c , with $D_c=180$ nm. The black line denotes the average D_p/D_c for each hour. The red line on the top of the graph denotes the normalized $dN/d\log D_p$ versus D_p/D_c for the clean period and polluted period before the tandem experiment.



1135

Figure 8. Diurnal variation in D_p/D_c for all periods, high O_x periods and low O_x periods. The gray shaded area denotes the standard deviation of D_p/D_c for all periods.

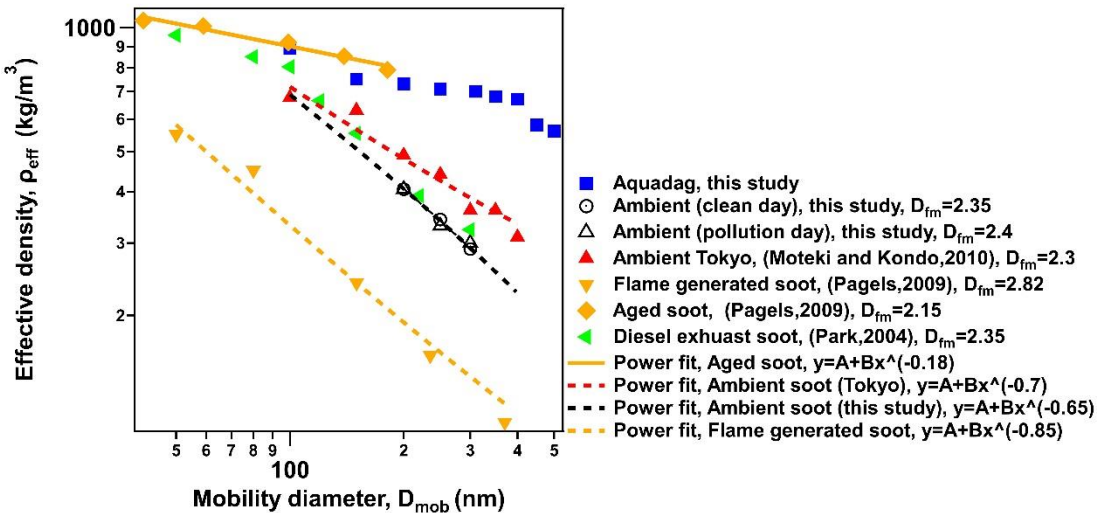


Figure 9. Relationship between effective density and mobility diameter of rBC-containing particles. The black circle and triangle denote the fresh rBC-containing particles ($D_p/D_c = 1$) measured on clean days and polluted days in this study. Other markers denote the data from previous research.

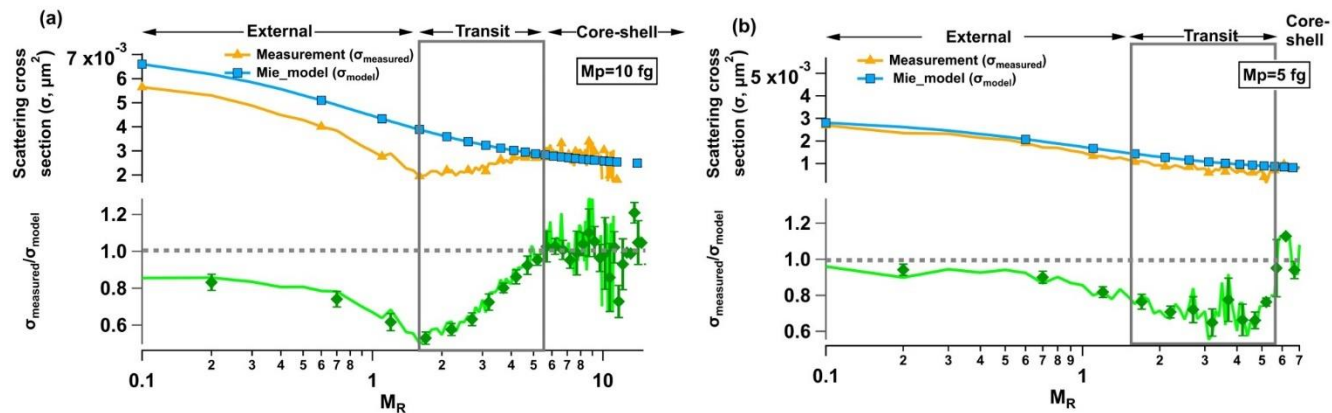


Figure 10. (a) Upper panel: scattering cross section of rBC-containing particles as measured by SP2 (yellow line) and calculated by Mie theory (blue line), assuming a core-shell structure. Bottom panel: the ratio (green line) between these two scattering cross sections at a CPMA setpoint of 10 fg as a function of M_R (the mass ratio of nonrefractory matter to rBC). (b) the same as (a) but for a CPMA setpoint of 5 fg.

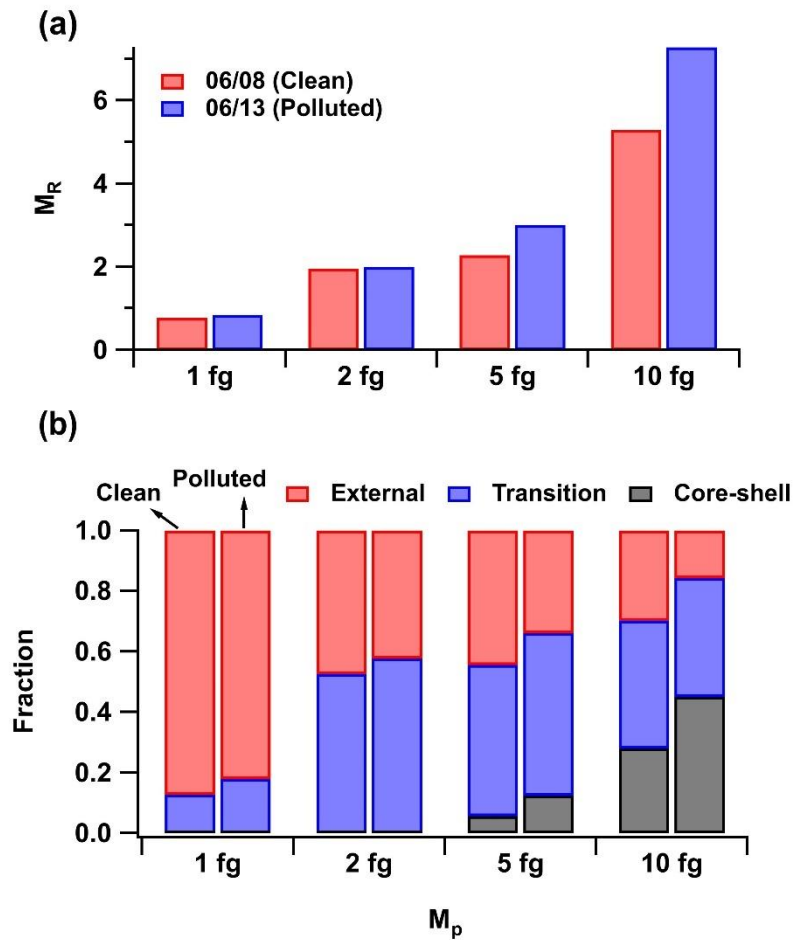
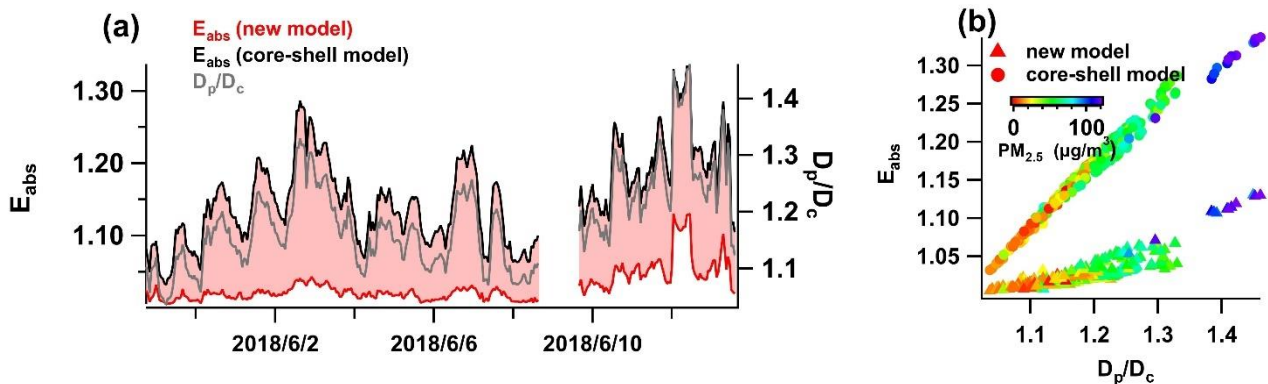


Figure 11. (a) The average M_R (the mass ratio of nonrefractory matter to rBC) under different CPMA setpoints (1 fg, 2 fg, 5 fg, 10 fg). (b) The fraction of different types of rBC-containing particles under different CPMA setpoints under varied pollution conditions.



1155

Figure 12. (a) Time series of D_p/D_c with $D_c=180\pm 10$ nm and E_{abs} at 550 nm wavelength with $D_c=180\pm 10$ nm using the core-shell model and the morphology-dependent model. (b) Relationship between E_{abs} and D_p/D_c . Circles denote the E_{abs} derived from the core-shell model, and triangles denote the E_{abs} derived from the morphology-dependent model.

1160

Mixing characteristics of refractory black carbon aerosols determined by a tandem CPMA-SP2 system at an urban site in Beijing

Supplementary

Table S1. Abbreviations and symbols used in this paper

Abbreviation/symbols	Full name/explanation
SP2	Single particle soot photometer (DMT Technologies)
DMA	Differential mobility analyzer (TSI Inc.)
CPMA	Couette centrifugal particle mass analyzer (Cambustion, Ltd.)
CPC	Condensation particle counter (TSI Inc.)
rBC	Refractory black carbon determined by SP2 through laser-induced incandescence method
D_c	Mass equivalent diameter of rBC core
MMD	Mass median diameter
D_p	Diameter of rBC-containing particles including rBC core and coatings
LEO	Leading-edge-only fitting method
M_p & M_{coat} & M_{rBC}	Mass of rBC-containing particles, mass of coating material, mass of rBC
M_R	M_{coat}/M_{rBC}
D_{mob}	Mobility diameter determined by DMA
ρ_{eff}	Effective density
D_{fm}	Mass fractal dimension
E_{abs}	Absorption enhancement of rBC-containing particles compared to bare rBC
$\sigma_{measured}$	Scattering cross section of rBC-containing particles measured by SP2
σ_{model}	Scattering cross section of rBC-containing particles calculated using the Mie theory

1165

Section 1 Calibration

Figure S1: The calibration of the incandescence channel. The data of incandescence peak and rBC mass is fitted using a poly function ($y = ax^2+bx+c$). The coefficient of the poly function varied little (<2%) before and after the observation indicating the stability of the incandescence channel. The scatter of incandescence intensity caused 25% uncertainty, resulting in an uncertainty of the derived BC mass of 20%, which causes an uncertainty of mass equivalent diameter of ~6%.

1170

Figure S2: The calibration of the scattering channel. The calibration factor varied little (<3%) before and after the observation indicating the stability of the scattering channel. The calibration is done using PSL with multiple sizes (203 nm, 240 nm 300 nm, 400 nm) before the observation. And the calibration is done only with PSL with 240 nm after the observation.

1175

Figure S3: The calibration curve for the detection efficiency of SP2. For rBC with diameter > 70 nm, the detection efficiency is larger than 80%.

1180

Figure S4: The calibration of the DMA-SP2 system. An DMA-SP2 system can determine the effective density of rBC. We test our DMA-SP2 system by measuring the effective density of aquadag and comparing the result with previous research. Our results are ~7% higher than the poly-fit of Gysel but lower than the results from Moteki and Kondo. These differences may be result of different characteristics of Aquadag with varied lot and different instrument condition (such as the uncertainty of SP2).

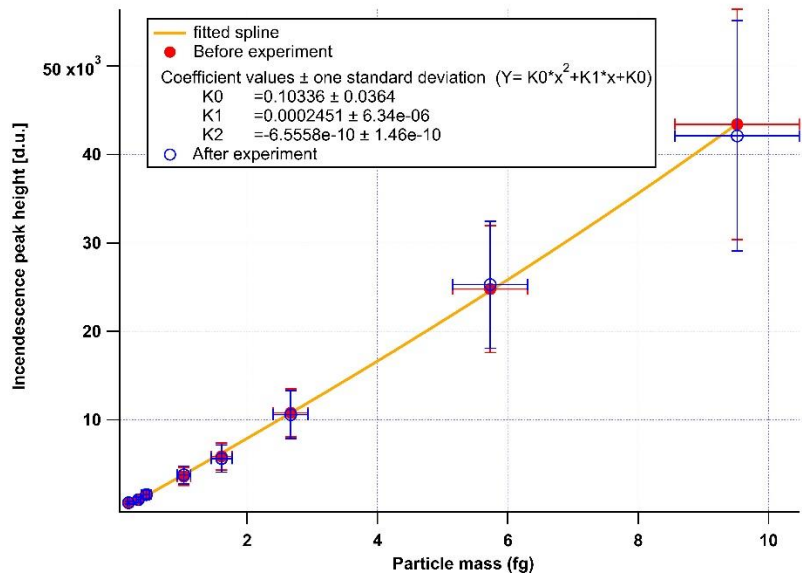


Figure S1 Calibration curve for incandescence broadband high gain channel.

1185

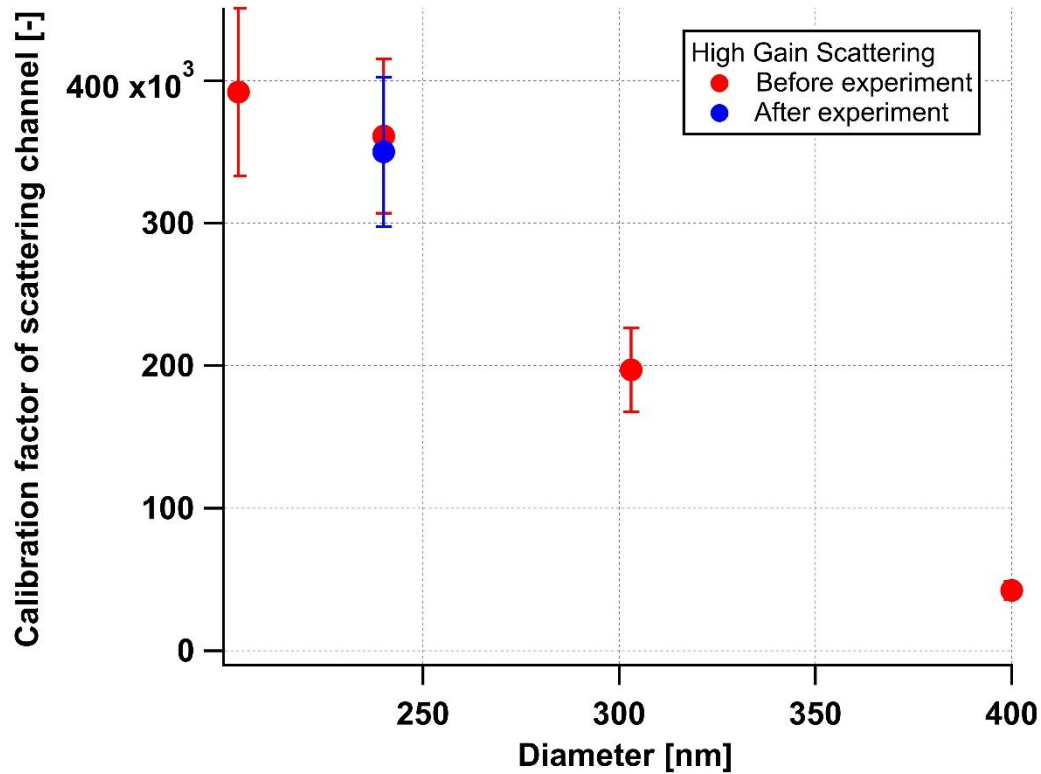
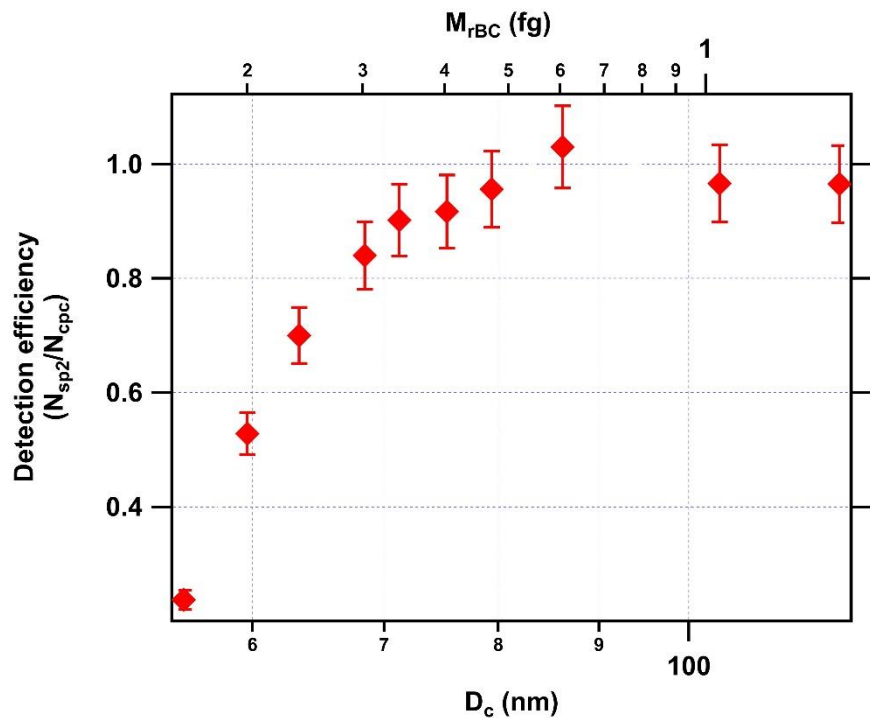


Figure S2 PSL calibration for high gain scattering channel before and after the investigation.



1190 Figure S3 Calibration curve for SP2's detection efficiency.

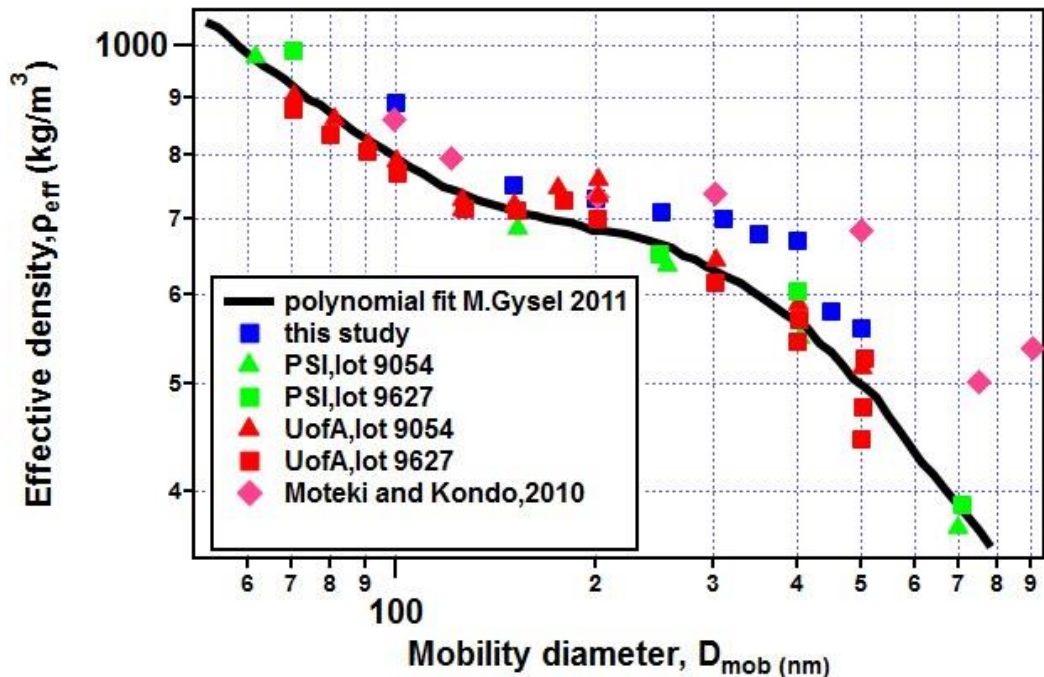


Figure S4 Relationship between effective density and mobility diameter of Aquadag measured in the present study and in previous studies.

1195

Section 2 Backward trajectory

An WRF-Flexpart model (<https://www.flexpart.eu>) was used to analyze where the air mass was from. The $1^\circ \times 1^\circ$ FNL data (rda.ucar.edu/) was used as the input meteorological data to WRF. WRF can produce meteorological data with higher resolution which was used as the input data for Flexpart. Air samples were released at 100m above ground level at the observation site (longitude: 116.37°E ; latitude: 39.97°N) and the simulation time of backward trajectory is 3 days.

1200 On the clean days (06/07, 06/08) the air mass was from the north of Beijing where there is little pollutant emission. Since the north air mass is clean, the local emitted pollutant may be dominant.

1205 On the pollution day (06/12, 06/13), the air mass was majorly from the south polluted area. The pollutant transportation may play an important role in pollution day.

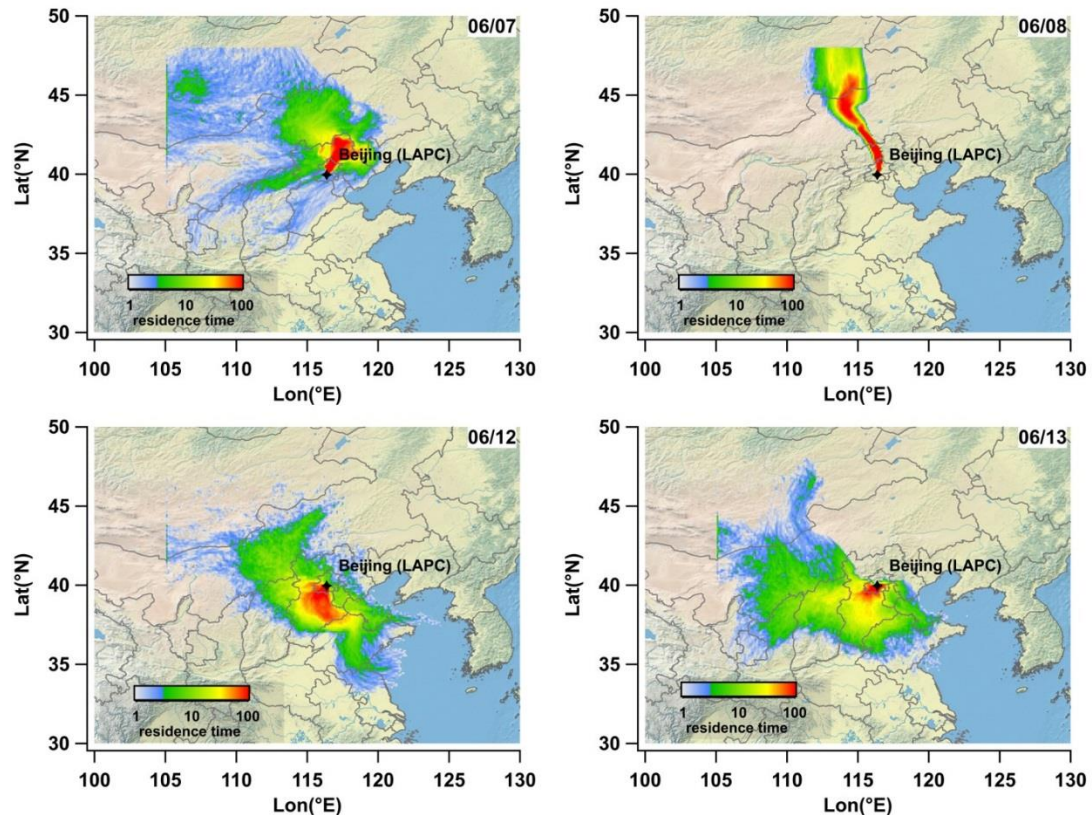


Figure S5 The backward trajectories at clean days (06/07, 06/08) and polluted days (06/12, 06/13), the map is the
 1210 built-in map of the IGOR software (<https://www.wavemetrics.com/>).

Section 3 Absorption enhancement calculation

1215 3.1 Description of morphology-dependent model

The absorption enhancement (E_{ab}) of a single rBC-containing particle is calculated as the ratio of absorption cross section of rBC-containing particle ($C_{abs,p}$) and absorption cross section of rBC core ($C_{abs,rBC}$) using Mie theory assuming a core-shell structure with refractive indices of 2.26+1.26i for rBC core and 1.48 for coatings.

$$E_{abs_coreshell} = \frac{C_{abs,p}}{C_{abs,rBC}}$$

1220 Considering rBC-containing particle is not in an ideal core-shell structure as discussed in section 4.1.2, the rBC-containing particles was classified into external, transition and core-shell stage based on the M_R range. The rBC-containing particles with an external mixing state were considered to have no absorption enhancement, and the rBC-containing particles at the core-shell stage were considered to have a core-shell structure and the same E_{abs} from Mie-theory under the assumption of a perfect core-shell structure. The E_{abs} in the transition period was calculated by the interpolation of E_{abs} between the external and
1225 internal stage, which can be explained as the following equation:

$$E_{abs_new} = \begin{cases} 1 & \text{when } M_R \leq 1.5 \\ \frac{E_{abs_coreshell}(M_R=6) - E_{abs_coreshell}(M_R=1.5)}{6-1.5} * (M_R - 1.5) + 1 & \text{when } 1.5 < M_R < 6 \\ E_{abs_coreshell} & \text{when } M_R \geq 6 \end{cases}$$

The reliability of this morphology- dependent model has been proven by comparing the E_{abs} derived from the model and measuring the E_{abs} (Liu et al., 2017).

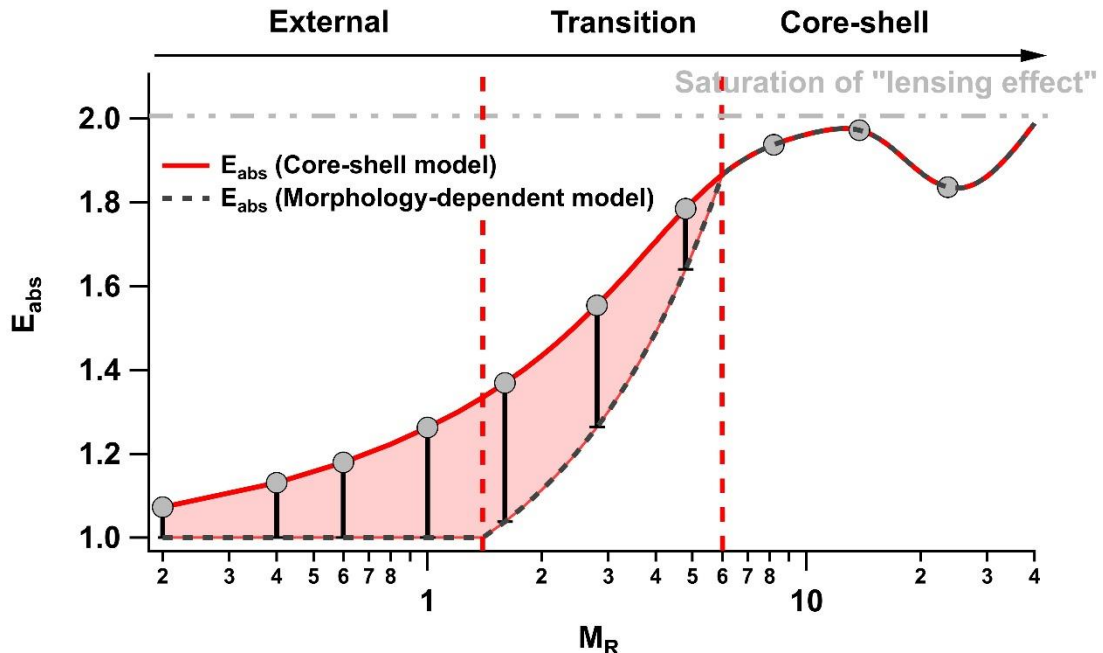


Figure S6 Dependence of E_{abs} on M_R at wavelength of 550 nm and $D_c = 180$ nm, calculated using the Mie model under the assumption of a core-shell structure (red solid line). The gray dashed line denotes the E_{abs} calculated from morphology-dependent model.

1235

3.2 Applying the morphology-dependent model

The D_p and D_c can be directly obtained in the single SP2 measurement. With the rBC density of 1.8 g/cm³ and assuming a coating density of 1.5 g/cm³, the M_R of every single rBC-containing particle can be calculated in the ambient measurement. Thus, the relationship of the morphology-dependent model between M_R and E_{abs} can be used. We calculated the E_{abs} of every 1240 single rBC-containing particle with $D_c = 180$ nm in one hour and reported the average E_{abs} in Fig. 12.